Spin-Orbit Charge Recombination Intersystem Crossing in Phenothiazine–Anthracene Compact Dyads: Effect of Molecular Conformation on Electronic Coupling, Electronic Transitions and Electron Spin Polarizations of the Triplet States

Yuqi Hou,[a] Till Biskup,[b] Stephan Rein,[b] Zhijia Wang,[a] Laura Bussotti,[c] Nino Russo,[d] Paolo Foggi,[c,e,f] Jianzhang Zhao [a,] Mariangela Di Donato,[c,e,]* Gloria Mazzone [d,]* and Stefan Weber [b,]**

[a] State Key Laboratory of Fine Chemicals, School of Chemical Engineering, Dalian University of Technology, E–208 West Campus, 2 Ling Gong Rd., Dalian 116024, China. E-mail: zhaojzh@dlut.edu.cn

[b] Institute of Physical Chemistry, Albert-Ludwigs-Universität Freiburg, Albertstr. 21, 79104 Freiburg, Germany. E-mail: stefan.weber@physchem.uni-freiburg.de

[c] LENS (European Laboratory for Non-Linear Spectroscopy), Via N. Carrara 1, I-50019 Sesto Fiorentino, Italy. E-mail: didonato@lens.unifi.it

[d] Dipartimento di Chimica e Tecnologie Chimiche, Università della Calabria, I-87036 Arcavacata di Rende, Italy. E-mail: gloria.mazzone@unical.it

[e] INO, Istituto Nazionale di Ottica, Largo Enrico Fermi 6, I-50125 Florence, Italy.

[f] Department of Chemistry, Biology and Biotechnology University of Perugua, Via Elce di Sotto 8, I-06123 Perugia, Italy.

Abstract: Phenothiazine (PTZ)–Anthracene (An) compact electron donor/acceptor dyads were synthesized. The molecular conformation was constrained by rotation restriction to achieve an orthogonal geometry between the electron donor (PTZ) and the electron acceptor (An), with the aim to enhance the spin-orbit charge-transfer intersystem crossing (SOCT-ISC). The substitution positions on the PTZ and An moieties were varied to attain dyads with different mutual orientation of the donor/acceptor as well as different rotation-steric hindrance. The electronic coupling strengths between the electron donor and the acceptor were quantified with the matrix elements (V_{DA}, 0.04 – 0.18 eV); the smallest value was observed for the dyad with orthogonal geometry. Charge-transfer absorption and fluorescence emission bands were observed for the dyads, for which the intensity varied based on the V_{DA} values. The fluorescence of the An moiety was significantly quenched in the dyads, efficient ISC and the formation of triplet state were confirmed with nanosecond transient absorption spectroscopy (Φ_{Δ} = 65%, τ_T = 209 μs). The rotation-steric hindrance was analyzed with potential energy curves and PTZ was found to be an ideal electron donor to attain SOCT-ISC. Time-resolved electron paramagnetic resonance (TREPR) spectra revealed the electron-spin polarization (ESP) of the triplets of the dyads, which is drastically different from that of anthracene, thus confirming the SOCT-ISC mechanism. Moreover, we found that the ESP patterns of the dyads strongly depend on the topological features of the molecules and the structure of the electron donor, thus indicating that the relationship between the molecular conformation and the ESP parameters of the triplet state of the dyads cannot be described solely by the orthogonal geometry, as was previously suggested.

1. INTRODUCTION

Controlling the electronic excited states of chromophores is crucial to developing functional organic molecular materials that are suitable as molecular probes,[1] charge separation systems for

photovoltaics or photocatalysis,[2–4] fluorescent molecular probes,[5–6] molecular logic gates or switches,[7] activatable (or targeted) photodynamic therapeutic reagents,[7–10] or external stimuli–responsive triplet-triplet annihilation (TTA) upconversion.[11–15]

A few typical strategies have been studied to tune the excited states of organic chromophores. The most straightforward way is to modify the π-conjugation framework by introducing electron-donating or -withdrawing substituents on the π-conjugation moiety,[16–18] which will induce changes in the UV–Vis absorption, luminescence and the redox properties of the chromophore. Another method is to construct supramolecular chromophore systems with different components, such as light-harvesting systems based on Förster-resonance-energy transfer (FRET),[19–21] or dyads or polyads with charge-separation (CS) ability upon photoexcitation.[22–28] In an ideal situation, for the π-conjugation framework, the different moieties in the molecule are electronically fully *coupled*, even in the ground state. For the latter, however, the components are fully *decoupled* at ground state under ideal circumstances.

Recently, as an alternative to the above-mentioned two typical approaches of tuning the electronic excited states of chromophores by full coupling or decoupling, dyad (or polyad) systems, in which the two components (very often an electron donor and an electron acceptor) are *weakly coupled* have attracted considerable attention.[22,23,29–33] The electronic coupling can be quantified by the electronic coupling matrix element (V_{DA});[34–36] the magnitude of this value is normally manifested by the intensity of the charge transfer (CT) bands in UV–Vis absorption and/or luminescence spectra of the compounds.[37–41]

In systems with moderate V_{DA} values, new spectral features are often observed as compared to the individual chromophores, for instance, the occurrence of CT absorption or luminescence bands.[37–39,42] Weakly coupled systems could furthermore develop interesting properties, for

instance thermally-activated delayed fluorescence (TADF).[43–45] In molecules that exhibit TADF, a *delicately* balanced electronic coupling between the electron donor and the acceptor must be attained to keep the electron exchange energy (J) small, but at the same time to make the radiative transition from the CT emissive state efficient.[46,47] Investigating the relationship between V_{DA} and the photophysical properties of organic molecules is an interesting topic, but up to now, research in this area is to a large extent limited to studies of the formation of CT states.[22,23,38,48] The radiative decay of the CT state, especially the formation of triplet states by charge recombination (CR) were rarely investigated.[24,31,49,50]

Concerning the above-mentioned aspects, a chromophore attached to an electron donor (or acceptor) with moderate coupling between the components is of particular interest. Different from the molecular structure profiles with fully coupled or decoupled components, moderate coupling between electron donor/acceptor will result in singlet-state energy levels different from the chromophore itself. Furthermore, recently it was shown that in weakly coupled multi-chromophore systems, intersystem crossing (ISC) can be induced through CR, especially in cases where the two moieties are arranged in an *orthogonal* conformation. In this situation, the electron transfer between the poorly overlapped molecular orbitals will cause molecular orbital angular momentum change, thus generating a magnetic torque to flip the electron spin. In other words, the electron spin moment change during the ISC (spin rephrasing or flip) will be compensated by the change of molecular orbital momentum.[37] Under such circumstance the ISC is greatly facilitated, with the so-called spin-orbit charge-transfer (SOCT) process.[37,42,51–56] SOCT-ISC is different from the conventional CR-induced ISC process (very often via a radical pair mechanism, through the Zeeman and hyperfine coupling interactions).[29,57]

The relationship between the SOCT-ISC efficiency and the electronic coupling, the molecular geometry and the structure of the electron donor/acceptor, is far from being fully understood. It was recently found that the ISC efficiency is greatly enhanced in case of julolidine/anthracene dyads with orthogonal geometry, as compared to analogous systems showing less rotation restrictions and a more coplanar geometry.[37] It was proposed that a higher triplet state with similar energy to the CT state is mandatory for efficient SOCT-ISC, but more examples are needed to confirm this postulation. Although previously the coupling between a dialkylamine and an anthracene unit was studied with variation of the conformation restriction on the dialkylamine, the formation of triplet states was not studied.[39]

Herein, we constructed several dyads with the aim to understand the structure-function relationships in a few SOCT-ISC systems. We selected phenothiazine (PTZ) as electron donor and anthracene (An) as electron acceptor to construct compact electron-donor–anthracene dyads (Scheme 1). The connection (C–C or C–N bonds) between the two moieties was varied such as to systematically tune the geometry constraint (rotation hindrance), which will reflect in different electronic coupling strengths (V_{DA}), subsequently affecting the photophysical properties, in particular the triplet state quantum yields. We observed that the fluorescence of the anthracene moiety is significantly quenched in the dyads, and high ISC quantum yields (ca. 80%) are attained. We postulate that SOCT plays a significant role in ISC. This postulate is corroborated by time-resolved electron paramagnetic resonance (TREPR) data, in which electron spin polarization (ESP) was revealed for the triplet excited state of the dyads. We found that the ESP phase and the population ratio of the triplet sublevels (T_+, T_0, and T_-) strongly depend on the topological features of the dyads. Radical-pair ISC (RP-ISC) is unlikely for these compact electron donor/acceptor dyads, due to the strong electron exchange interaction (J).

2. EXPERIMENTAL SECTION

2.1. General method. Compounds 9,10-dibromo-9,10-dihydroanthracene, **PTZ-N-9An** and **DPA-9An** were synthesized according to methods reported in the literature.[37,58] All chemicals used are analytically pure grade and were used as received. Petroleum ether (boiling point: 60–90 °C) was used for column chromatography. Solvents were dried and distilled prior to use. UV−Vis absorption spectra were obtained on UV-2550 UV-VIS spectrophotometer (Shimadzu Ltd, Japan). Fluorescence spectra were measured on RF-5301PC spectrofluorometer (Shimadzu Ltd, Japan) Fluorescence lifetimes were measured on an OB920 (Edinburgh Instruments Ltd, UK) luminescence lifetime spectrometer.

2.2. Compound PTZ(2)-C-9An. Under N_2 atmosphere, 9,10-dibromo-9,10-dihydroanthracene (1.02 g, 3.57 mmol) was dissolved in dry chloroform (20 mL, ethanol free). The mixture was cooled to 0 ºC, and a *N*-*n*-butyl-phenothiazine (1.54 g, 6.0 mmol) solution in chloroform (5 mL) was added dropwise over 35 min. After stirring for another 2.5 h at 0 ºC, the mixture was stirred overnight at room temperature. The solvent was removed under reduced pressure, and the residue was purified with column chromatography (silica gel, petroleum ether/CH_2Cl_2= 1/3, v/v) to give a yellowish solid (40 mg, yield 3.0%). ^{1}H NMR ($CDCl_3$, 400 MHz): δ 8.47 (s, 1H), 8.03 (d, 2H, J = 8.5 Hz), 7.73 (d, 2H, J = 8.7 Hz), 7.47–7.33 (m, 4H), 7.23–6.98 (m, 7H), 3.97 (s, 2H), 1.96–1.89 (m, 2H), 1.60–1.50 (m, 2H), 1.04–1.00 (t, 3H). ^{13}C NMR ($CDCl_3$, 100 MHz): δ 145.09, 144.77, 136.04, 132.75, 131.39, 130.40, 130.20, 129.96, 128.32, 127.59, 127.34, 126.91, 126.56, 125.35, 125.12, 124.78, 122.52, 115.51, 115.08, 47.33, 29.73, 29.20, 20.38, 13.95. MALDI–HRMS: Calcd ($[C_{30}H_{25}NS]^+$), m/z = 431.1708; found, m/z = 431.1681.

2.3. Compound PTZ-N-9An. Under N_2 atmosphere, phenothiazine (56 mg, 0.28 mmol), 9-bromoanthracene (64 mg, 0.25 mmol), $Pd_2(dba)_3$ (3% mol), P*t*Bu_3 (6% mol), NaO*t*Bu (5 eq.)

were mixed in 1,4-dioxane (5 mL). The mixture was stirred for 11 h at 100 ºC. After the reaction, the mixture was extracted with dichloromethane (3 × 15 mL) and washed with brine, dried over anhydrous Na_2SO_4. The solvent was evaporated under reduced pressure, the crude product was purified by column chromatography (silica gel, petroleum ether) to give a yellowish solid (12 mg, yield 13%). ^{1}H NMR ($CDCl_3$, 400 MHz): δ 8.63 (s, 1H), 8.29 (d, 2H, J = 9.6 Hz), 8.14 (d, 2H, J = 7.4 Hz), 7.55–7.48 (m, 4H), 7.05 (d, 2H, J = 7.6 Hz), 6.73–6.58 (m, 4H), 5.73 (s, 2H). MALDI–HRMS: Calcd ($[C_{26}H_{17}NS]^+$), m/z = 375.1082; found, m/z = 375.1096.

2.4. Compound PTZ-N-2An. Under N_2 atmosphere, phenothiazine (200 mg, 1.0 mmol), 2-bromoanthracene (384 mg, 1.5 mmol), $Pd_2(dba)_3$ (3% mol), P*t*Bu$_3$ (6% mol), NaO*t*Bu (3 eq.) were mixed in toluene (5 mL). The mixture was stirred for 11 h at 100 ºC. After the reaction, the mixture was extracted with dichloromethane (3 × 15 mL) and washed with brine, dried over anhydrous Na_2SO_4, and the solvent was evaporated under reduced pressure. The crude product was purified by column chromatography (silica gel, petroleum ether) to give a yellowish solid (220 mg, yield 59%). ^{1}H NMR ($CDCl_3$, 400 MHz): δ 8.53 (s, 1H), 8.45 (s, 1H), 8.23 (d, 1H, J = 8.9 Hz), 8.07–8.01 (m, 3H), 7.53–7.51 (m, 2H), 7.44–7.42 (d, 1H, J = 8.9 Hz), 7.07–7.05 (m, 2H), 6.84–6.82 (m, 4H), 6.34–6.31 (m, 2H). TOF–HRMS: Calcd ($[C_{26}H_{17}NS]^+$), m/z = 375.1082; found, m/z = 375.1093.

2.5. Compound DPA-9An. Under N_2 atmosphere, diphenylamine (169 mg, 1 mmol), 9-bromoanthracene (384 mg, 1.5 mmol), $Pd_2(dba)_3$ (3% mol), P*t*Bu$_3$ (6% mol), NaO*t*Bu (3 eq.) were mixed in toluene (5 mL). The mixture was stirred for 11 h at 100 ºC. After the reaction, the mixture was extracted with dichloromethane (3 × 15 mL) and the organic layer was washed with brine, dried over anhydrous Na_2SO_4. The solvent was evaporated under reduced pressure, and finally the crude product was purified by column chromatography (silica gel, petroleum ether) to

give a yellowish solid (80 mg, yield 23%). ^{1}H NMR ($CDCl_3$, 400 MHz): δ 8.50 (s, 1H), 8.12–8.05 (m, 4H), 7.46–7.36 (m, 4H), 7.17–7.13 (m, 4H), 7.07–7.05 (m, 4H), 6.88–6.85 (m, 2H). TOF–HRMS: Calcd ($[C_{26}H_{19}N]^+$), m/z = 345.1517; found, m/z = 345.1519.

2.6. Nanosecond Time-Resolved Transient Absorption Spectra. The nanosecond transient absorption spectra were measured on a LP980 laser flash photolysis spectrometer (Edinburgh Instruments, UK). A collinear mode was used in the measurement to enhance the signal-to-noise ratio. The signal was digitized on a Tektronix TDS 3012B oscilloscope, and the data were analyzed using the L900 software.

2.7. Femtosecond Time-Resolved Transient Absorption Spectra. Transient absorption spectra (TAS) with 150-fs time resolution were acquired on a system based on a Ti:sapphire regenerative amplifier (BMI Alpha 1000) pumped by a Ti:sapphire oscillator (Spectra Physics Tsunami). The system produces 100-fs pulses at 785 nm, with a repetition rate of 1 kHz and average power of 450–500 mW, and excitation pulses at 390 nm by second-harmonic generation of the fundamental laser output through a BBO crystal. The probe pulses were generated by focusing a small portion of the fundamental laser output radiation on a 3 mm thick calcium fluoride window. The pump beam polarization has been set to the magic angle with respect to the probe beam by rotating a λ/2 plate. Pump-probe delays were introduced by sending the probe beam through a motorized stage. Multichannel detection was achieved by sending the white light continuum after passing through the sample to a flat field monochromator coupled to a home-made CCD detector [http://lens.unifi.it/ew]. TAS measurements were carried out in a quartz cell (2 mm thick) mounted on a movable stage to avoid sample photo-degradation and multiple-photon excitation. The recorded kinetic traces and transient spectra have been analyzed by using a global-analysis procedure.[59] The number of kinetic components has been estimated by

performing a preliminary singular values decomposition (SVD) analysis.[60] Global analysis was performed using the GLOTARAN package (http://glotaran.org),[61] employing a linear unidirectional ("sequential") model.

2.8. Time-Resolved Electron Paramagnetic Resonance (TREPR) Spectroscopy. All TREPR experiments were performed at 80 K using a setup described previously.[62,63] Optical excitation at 355 nm was carried out using a Nd:YAG laser GCR 190-10 (Spectra Physics, Santa Clara, CA). The repetition rate of the laser was set to 10 Hz (pulse duration: 10 ns) at an energy of 1 mJ per pulse. A Bruker ESP-300 (Bruker, Rheinstetten, Germany) spectrometer was used in combination with a Bruker ER046 MRT (Bruker, Rheinstetten, Germany) microwave bridge. The samples were placed in synthetic quartz tubes (Ilmasil PS, Qsil GmbH, Langewiesen, Germany) with inner diameter of 3 mm, and irradiated in a dielectric-ring resonator ER 4118-MD5 (Bruker, Rheinstetten, Germany). The resonator was immersed into a CF935 (Oxford Instruments, Oxford, UK) helium-gas flow cryostat and the temperature stabilized by a temperature controller ITC503 (Oxford Instruments, Oxford, UK). The microwave power was set to 2 mW and the microwave frequency read out by a frequency counter 5352B (Hewlett-Packard, Böblingen, Germany). Signal acquisition was performed with a transient recorder 9354A (LeCroy, Chestnut Ridge, NY) at an overall detection bandwidth of 25 MHz. Distortions of the signal baseline introduced by the laser pulse were corrected by subtracting a signal collected at an off-resonant magnetic-field position.

2.9. DFT Calculations. Geometry optimizations and calculations of absorption spectra of the compounds were performed at the density functional theory (DFT) and its time-dependent extension (TDDFT) levels, respectively. To select the best protocol, several exchange and correlation functionals, B3LYP,[64,65] cam-B3LYP,[66] M06, M06L, M062X,[67] B97D,[68] ωB97XD,[69]

PBE,[70] PBE0[71] and LC-ωPBE,[72,73] were employed and coupled with the 6-31G** basis set on computing absorption spectrum of **DPA-9An**, optimizing the structure at each level. No imaginary frequencies were found for all optimized structures. The environment, toluene (ε = 2.37), was taken into account by means of the integral equation formalism of polarizable continuum model (IEFPCM).[74] The excitation energies and the energy gaps between the S_0 state and the excited states of the compounds were approximated based on the ground-state equilibrium geometry at the TDDFT level. All these calculations were performed with Gaussian 09W.[65,75] Based on the outcomes of benchmark studies on **DPA-9An**, the PBE0 functional was selected, as it provides the best agreement with the experimental absorption bands.

Spin-orbit matrix elements were computed with the DALTON code[76] using the atomic-mean-field approximation[77] and following the procedure reported previously.[78] For this purpose, B3LYP has been employed in combination with the cc-pVDZ basis set for all atoms.

3. RESULTS AND DISCUSSION

3.1. Design and Synthesis of the Compounds. As electron donor, phenothiazine (PTZ) was used for synthesis of the dyads (Scheme 1).[26–28,31,33,79,80] PTZ forms a stable radical cation upon electron transfer. This moiety has been used previously in studies of SOCT-ISC.[55] For comparison with the previous studies, anthracene (An) was selected as electron acceptor and visible light-absorbing chromophore in the current dyads (Scheme 1).[37] Three dyads with different linkage between the two chromophores were synthesized (Scheme 1). In **PTZ(2)-C-9An**, the C–C connection is at the 2- and 9-positions of PTZ and An, respectively. For **PTZ-N-9An** and **PTZ-N-2An**, the 9- or 2-positions of the An moiety form a C–N bond with PTZ, respectively. We envisaged an orthogonal geometry for the two moieties in **PTZ-N-9An,** due to the steric hindrance generated by the rotation about the linker. In **PTZ(2)-C-9An** and **PTZ-N-**

2An the steric hindrance between the two moieties is expected to be smaller. **DPA-9An** was used as a reference compound. We note that recently an analogue to **PTZ-N-9An** was reported, which has an extra phenyl substituent at the anthracene unit.[48] However, the previous study of the analogue PTZ–An was focused on tuning the CT state energy level and its application in electroluminescence, but not on triplet states.

Scheme 1. Synthesis of the Compounds [a]

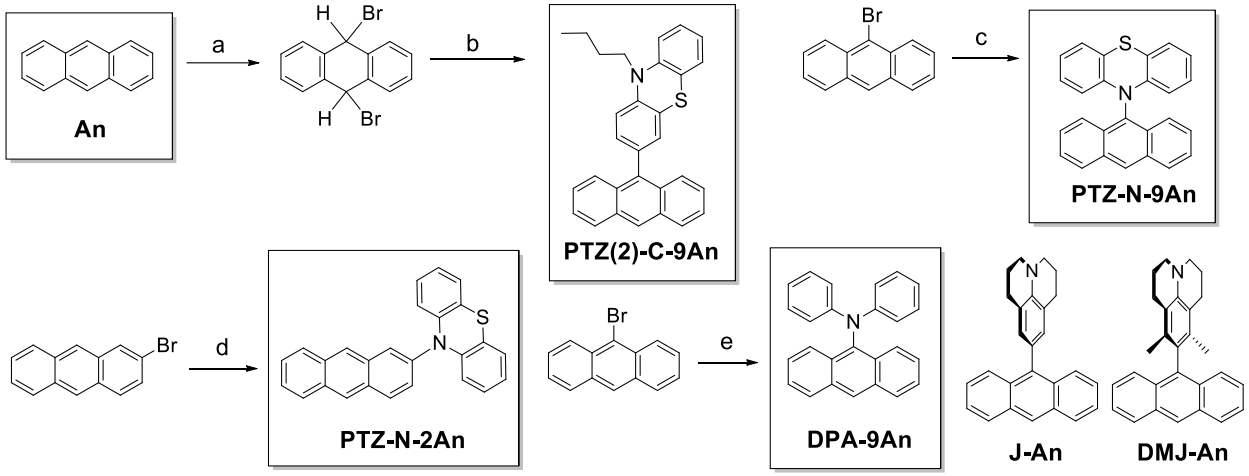

[a] Key: (a) Under N_2, Br_2, CS_2, 0 ºC, 30 min; (b) Under N_2, chloroform (ethanol-free), *N*-butylphenothiazine, 0 ºC to room temperature, overnight; yield: 3.0%; (c) under N_2, phenothiazine, $Pd_2(dba)_3$, P*t*Bu$_3$, NaO*t*Bu, 1,4-dioxane, 100 ºC, 11 h; yield: 13%; (d) similar to (c), yield: 59%; (e) similar to (c), yield: 23%.

Based on the Buchwald-Hartwig coupling reaction, **PTZ-N-9An**, **PTZ-N-2An** and **DPA-9An** were synthesized and the overall yields are moderate (more than 10%). **DPA-9An** and **PTZ-N-9An** were reported previously but their photophysical properties were not studied.[39,58] An analogue of **PTZ(2)-C-9An**, with a different alkyl chain on the nitrogen atom, was studied for synthesis methodology, but the photophysical properties were not studied.[81] The molecular structures of all compounds were verified with ^{1}H NMR and HR MS spectra.

3.2. UV–Visible Absorption and Fluorescence Emission Spectra. UV–Vis absorptions of the compounds are shown in Figure 1. Due to the steric hindrance in **PTZ-N-9An**, we assume that the two components adopt an orthogonal geometry, thus the electronic coupling between the phenothiazine and the anthracene moieties in **PTZ-N-9An** should be weak.[37,39] On the other hand, **PTZ(2)-C-9An** is anticipated to be in a coplanar geometry, thus the electronic coupling between the PTZ and An moieties will be stronger than that in **PTZ-N-9An**. This is in agreement with the rotation potential energy studies (see later section).

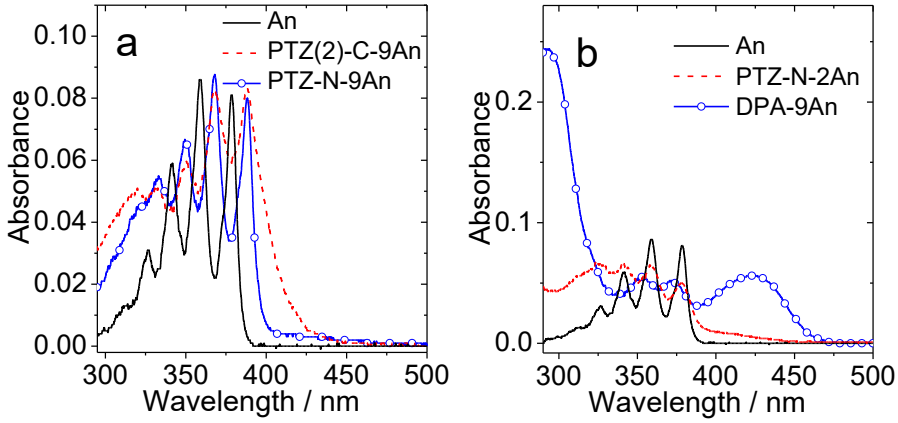

Figure 1. UV–Vis absorption spectra of (a) **An**, **PTZ(2)-C-9An** and **PTZ-N-9An**, (b) **An**, **PTZ-N-2An** and **DPA-9An**. $c = 1.0 \times 10^{-5}$ M in toluene, 20 °C.

The absorption bands of **PTZ(2)-C-9An**, **PTZ-N-9An** and **PTZ-N-2An** in the short wavelength region represent the $S_0 \rightarrow {}^1L_a$ transition, which is localized on the An moiety (Figure 1a). The structured absorption band of **PTZ-N-9An** is similar to that of An, except for a red-shift and the appearance of a weak tailing CT absorption band. **PTZ(2)-C-9An** shows a broad shoulder at the red edge, which is assigned to a charge transfer (CT) absorption.[37,39,48] The CT absorption is more pronounced for **PTZ-N-2An**, where an absorption band in the 400–450 nm range is observed (Figure 1b), indicating the occurrence of stronger electronic coupling between

the PTZ and An moieties, due to the less restricted rotation around the C–N linker. For **DPA-9An**, a distinct CT absorption band is observed at 424 nm (Figure 1b).[39] The $S_0 \rightarrow {}^1L_a$ transitions of **DPA-9An** are different from the other compounds, indicating that the π-conjugation framework of the anthracene moiety is more significantly perturbed, due to the strong electronic coupling between the two moieties in **DPA-9An**.[39]

The magnitude of the CT band indicates the electronic coupling (V_{DA}) between the electron donor (PTZ) and the electron acceptor (anthracene). In **PTZ-N-9An**, the donor and acceptor are almost completely decoupled, due to the conformation restriction exerted by the steric hindrance of the rotation about the N–C linker. As such only a weak tailing CT band can be observed in the UV–Vis absorption spectrum. In **PTZ(2)-C-9An**, however, due to the reduced steric hindrance of the rotation about the C–C bond, the coupling becomes stronger, the tailing in the lower energy region of UV–Vis absorption spectrum is therefore more significant. It should be pointed out that for **PTZ-N-9An** and **PTZ-N-2An**, the rotational constraint of the cyclic structure of PTZ restricts the rotation around the N–C linker, and breaks the conjugation between nitrogen atom and anthracene, although both nitrogen atoms are directly attached to the anthracene moiety.[39] **DPA-9An** is without an extended cyclic structure for the electron donor. Thus, the π-conjugation between the electron donor and acceptor is significant, and as a result, a distinct CT band at 424 nm was observed for **DPA-9An** (Figure 1b).[39] The CT band of **PTZ-N-2An** is more significant than those of the previously reported DMJ–anthracene (DMJ: 4-(9-anthracenyl)-3,5-dimethyljulolidine) dyads.[37] For **PTZ-N-9An**, the absorption is similar to a previously reported DMJ–anthracene dyad, thus indicating weak coupling between the electron donor and the acceptor.[37]

To quantify the probability of the $S_0 \rightarrow {}^1CT$ transitions, the transition dipole moment M_{abs} was calculated using eq.1:[39]

$$\left|M_{\mathrm{abs}}\right|^2 = \frac{3\ln 10}{8\pi^3 N_{\mathrm{A}}} \frac{hc}{n\tilde{\nu}_{\mathrm{abs}}} \int_{\mathrm{band}} \varepsilon\left(\tilde{\nu}\right) d\tilde{\nu} \qquad \text{(eq. 1)}$$

where $\varepsilon(\tilde{\nu})$ [M^{-1} cm^{-1}] is the molar absorption coefficient on the wavenumber scale, $\tilde{\nu}_{abs}$ [cm^{-1}] the absorption maximum of the $S_0 \rightarrow {}^1CT$ band, h [erg s] Planck's constant, c [cm s^{-1}] the speed of light, n the refractive index of the solvent, and N_A [mol^{-1}] the Avogadro constant.

Table 1. Charge Transfer-Related Photophysical Parameters of the CT Band, Dipole Moments and Electronic Coupling Matrix Elements of the Compounds [a]

	$\tilde{\nu}_{abs}$ [b] / cm^{-1}	$\tilde{\nu}_F^{CT}$ [c] / cm^{-1}	M_{abs} [d] / D	M_F [e] / D	V_{DA}^F [f] / eV
PTZ(2)-C-9An	25900	20100	0.45	2.20	0.16
PTZ-N-9An	22600	– [g]	0.29	– [g]	– [g]
DPA-9An	23600	20400	1.84	1.78	0.18
PTZ-N-2An	25400	19000	0.86	0.50	0.04

[a] In toluene. The maxima and area of the $S_0 \rightarrow {}^1CT$ and $S_0 \leftarrow {}^1CT$ bands were evaluated by Gaussian fitting. [b] Absorption maximum, in wavenumbers. [c] Emission maximum, in wavenumbers. [d] Transition dipole moment of the $S_0 \rightarrow {}^1CT$ transition. [e] Transition dipole moment of the $S_0 \leftarrow {}^1CT$ transition. [f] Electronic coupling between the ground state and the CT state. [g] Not observed.

The fluorescence transition dipole moment and electronic coupling matrix element between donor and acceptor were calculated as follows:[23,39]

$$\left|M_{\mathrm{F}}\right|^2 = \frac{3hk_{\mathrm{r}}}{64\pi^4 \left(n\tilde{\nu}_{\mathrm{F}}^{\mathrm{CT}}\right)^3} \qquad \text{(eq. 2)}$$

$$V_{DA}^{F} = \left[\frac{1.4 \times 10^5 k_r}{n^3 R_c^2 \tilde{\nu}_F^{CT}} \right]^{1/2} \quad \text{(eq. 3)}$$

In eqs. 2 and 3, $\tilde{\nu}_F^{CT}$ (cm^{-1}) is the emission maximum of the CT band, k_r (s^{-1}) the radiative rate constant of the emission of the CT band, n the solvent refractive index, and R_c (Å) the center-to-center D–A distance, which was optimized by DFT calculations (R_c (**PTZ(2)-C-9An**) = 6.79 Å, R_c (**PTZ-N-9An**) = 5.88 Å, R_c (**DPA-9An**) = 5.16 Å, R_c (**PTZ-N-2An**) = 6.50 Å). The parameters are presented in Table 1 and Table 2.

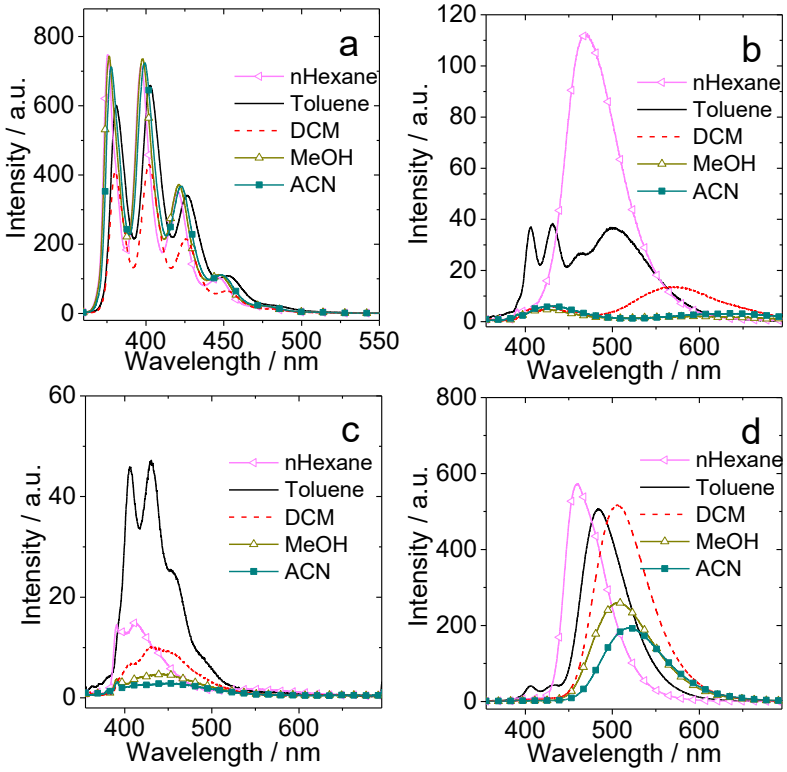

Figure 2. Fluorescence emission spectra of (a) **An**, (b) **PTZ(2)-C-9An**, (c) **PTZ-N-9An** and (d) **DPA-9An** in different solvents. Optically-matched solutions were used in each panel for direct comparison of the emission intensity (each of the solutions gives the same absorbance at the excitation wavelength, A = 0.050). λ_{ex} = 350 nm, 20°C.

Fluorescence emissions of the compounds were studied (Figure 2). The fluorescence band of **An** is structured, and both the emission intensity and the band positions are nearly solvent polarity-independent (Figure 2a). Interestingly, for the PTZ–An dyads, two emission bands were observed (Figure 2b). One is the structured locally excited (LE) emission band at 406 nm, the other emission band is the broad, structureless emission band at longer wavelengths around 500 nm.[39] The emission of **PTZ(2)-C-9An** in toluene gives two distinct bands at 406 nm (structured) and 501 nm (structureless) (Figure 2b). For **PTZ-N-9An**, a distinct LE emission band was observed in low-polarity solvents. And in *n*-hexane, a rather weak broad emission band was observed. However, in other solvents, even of high polarity, no obvious CT emission was observed (Figure 2c). These emission features indicate that the electronic coupling matrix elements, i.e., the V_{DA} value, is larger in **PTZ(2)-C-9An** than that in **PTZ-N-9An** (Table 1), for which no obvious CT emission was observed in toluene.

For **DPA-9An**, a weak LE emission band and one major structureless emission band were observed, indicating strong coupling between the two components in the excited state, and the emission arises from a singlet excited state with significant CT character. For **PTZ-N-2An**, similarly to **PTZ(2)-C-9An**, both structured and structureless emission bands were observed (Supporting Information, Figure S12), which indicates a stronger electronic coupling between the electron donor and acceptor. These results clearly demonstrate that the emission features are governed by the magnitude of the electronic coupling between the electron donor and acceptor within a dyad, and the latter can be controlled by modulating conformational restrictions.

The fluorescence excitation spectra (with the CT emission band set as the emission wavelength) of the dyads were analyzed (Supporting Information, Figure S14). The results show that the

excitation spectra are superimposable to the UV–Vis absorption spectra, suggesting that the ^{1}LE→^{1}CT transition is efficient.

The photophysical properties of the compounds are summarized in Table 2. The fluorescence quantum yields of the PTZ–An dyads (<10%) are much lower than those of dialkylaminophenyl–anthracene dyads.[39] This is due to the competition between CT and the radiative decay (fluorescence) from the S_1 state. Moreover, the occurrence of ISC may be another reason for the weak fluorescence of the electron donor/acceptor dyads (Table 2).

Table 2. Photophysical Properties of the Compounds [a]

	λ_{abs} / nm	ε [b]	λ_F / nm	τ_F [c] / ns	Φ_F [d] / %	k_r [e] / 10^7 s^{-1}	k_{nr} [f] / 10^7 s^{-1}	Φ_Δ [g] / %	Φ_T [h] / %
An	379	0.81	381	3.3	33	– [i]	– [i]	44, 50 [j], 70 [k]	37
PTZ(2)-C-9An	388	0.83	406, 501	4.0, 1.1 [l]	7.7, 4.6 [l]	4.14	86.0	56, 81 [j], 77 [k]	32
PTZ-N-9An	388	0.80	406	5.3	4.1	– [i]	– [i]	60, 65 [j], 59 [k]	34
DPA-9An	372, 424	0.51, 0.57	406, 484	4.3, 13.9 [l]	44, 39 [l]	2.81	4.39	39, 17 [j], 55 [k]	– [i]
PTZ-N-2An	378	0.50	406, 535	4.0, 4.4 [l]	4.8, 0.8 [l]	0.18	22.7	52, 66 [j], 36 [k]	34

[a] In toluene (1.0×10^{-5} M). [b] Molar extinction coefficient at the absorption maxima. ε : 10^4 M^{-1} cm^{-1}. [c] Fluorescence lifetime of the LE emission band. [d] Fluorescence quantum yield with anthracene as standard (Φ_F = 30% in ethanol). The estimated determination error is ±2%. [e] Radiative rate constant of the CT emission band. [f] Nonradiative rate constant of the CT emission band. [g] Singlet oxygen quantum yield ($^1O_2$) with $Ru(bpy)_3[PF_6]_2$ as standard (Φ_Δ = 57% in DCM) in toluene. The estimated determination error is ±2%. [h] Triplet quantum yield with anthracene as standard (Φ_T = 70% in ethanol) in toluene. The estimated determination error is ±2%. [i] Not observed. [j] In DCM. [k] In acetonitrile. [l] For the CT emission band.

The singlet oxygen quantum yields (and the triplet state quantum yields) of the PTZ–An dyads are comparable to those of anthracene,[82] thus we anticipate that the ISC of PTZ–An dyads is not exclusively caused by the intrinsic ISC of the anthracene moiety; other ISC channels, such as the

SOCT-ISC, must contribute to the ISC of the dyads. Because the fluorescence of the anthryl moiety in the dyads was strongly quenched, the direct $S_1 \rightarrow T_1$ ISC (T_2 state may be involved as a transient intermediate state) should be reduced. Our TREPR measurements (see below) confirm that the ISC mechanisms (SOCT-ISC) for the dyads are different from that of anthracene.

3.3. Electrochemical Studies: Cyclic Voltammetry and the Gibbs Free Energy Changes of the Photo-induced Charge Separation (ΔG_{CS}). In order to study the PET process, the electrochemical properties of the compounds were observed with cyclic voltammetry (Figure 3).

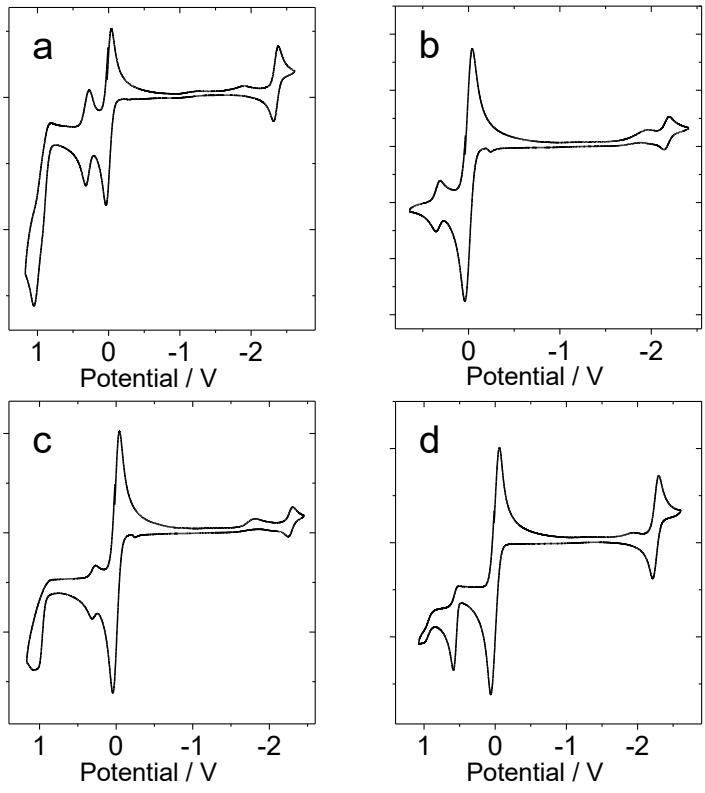

Figure 3. Cyclic voltammograms of (a) **PTZ(2)-C-9An**, (b) **PTZ-N-9An**, (c) **PTZ-N-2An** and (d) **DPA-9An** in deaerated acetonitrile containing 0.10 M $Bu_4N[PF_6]$ as supporting electrolyte and $Ag/AgNO_3$ as reference electrode. Scan rate: 100 mV/s. Ferrocene (Fc) was used as internal reference (set as 0 V in the cyclic voltammograms), $c = 5.0 \times 10^{-4}$ M, 20°C.

For anthracene, an irreversible oxidation wave at +0.90 V and a reversible reduction wave at –2.40 V were observed. For diphenylamine and phenothiazine, only oxidation waves were observed at +0.40 V, +0.56 V and +0.21 V, +0.54 V, respectively (Table 3). No reduction wave was observed under the experimental condition, indicating that diphenylamine and phenothiazine moieties are more likely to be as electron donors than acceptors.

Table 3. Redox Potentials of the Compounds [a]

Compounds	E_{RED} / V	E_{OX} / V
Anthracene	–2.40	+0.90
Diphenylamine	– [b]	+0.40, +0.56
Phenothiazine	– [b]	+0.21, +0.54
PTZ(2)-C-9An	–2.35	+0.30, +0.97
PTZ-N-9An	–2.17	+0.33
DPA-9An	–2.28	+0.58, +0.89
PTZ-N-2An	–2.25	+0.29, +1.05

[a] Cyclic voltammetry measurements in N_2-saturated acetonitrile containing a 0.10 M Bu_4NPF_6 supporting electrolyte. Redox potentials of the compounds were determined with Ferrocene (Fc) as the internal standard (0 V). Counter electrode is Pt electrode and working electrode is glassy carbon electrode, $Ag/AgNO_3$ couple as the reference electrode. [b] Not observed.

For the phenothiazine derivatives **PTZ(2)-C-9An**, **PTZ-N-9An**, and **PTZ-N-2An**, a reduction wave was observed, which is similar to that of anthracene (Figure 3). For **PTZ(2)-C-9An**, two oxidation waves at +0.30 and +0.97 V were observed and one reduction wave was recorded at –2.35 V. For **PTZ-N-9An**, one oxidation wave at +0.33 V was observed and one reduction wave at –2.17 V was recorded. For **PTZ-N-2An**, two oxidation waves at +0.29 and +1.05 V were observed, and one reduction wave was recorded at –2.25 V. For **DPA-9An**, two oxidation waves at +0.58 and +0.89 V were observed and one reduction wave was recorded at –2.28 V (Table 3).

The Gibbs free energy change (ΔG_{CS}) of the electron-transfer process was calculated using the Rehm-Weller equation (eq. 4),

$$\Delta G_{CS} = e[E_{OX} - E_{RED}] - E_{00} + \Delta G_S \quad \text{(eq. 4)}$$

$$\Delta G_S = -\frac{e^2}{4\pi\varepsilon_S\varepsilon_0 R_c} - \frac{e^2}{8\pi\varepsilon_0}\left(\frac{1}{R_D} + \frac{1}{R_A}\right)\left(\frac{1}{\varepsilon_{REF}} - \frac{1}{\varepsilon_S}\right) \quad \text{(eq. 5)}$$

$$E_{CS} = e\left[E_{OX} - E_{RED}\right] + \Delta G_S \quad \text{(eq. 6)}$$

in which ΔG_S is the static Coulombic energy, which is described by eq. 5. In eq.4 and 5, e is the electronic charge, E_{OX} is the half-wave potential for one-electron oxidation of the electron-donor unit (for irreversible oxidation, the anodic peak potential was used instead of the half-wave potential), and E_{RED} is the half-wave potential for one-electron reduction of the electron-acceptor unit, E_{00} is the energy level approximated with the crossing point of the normalized UV–Vis absorption and fluorescence emission spectra of the singlet excited state (LE state), in acetonitrile solution, ε_S is the static dielectric constant of the solvent, R_c is the center-to-center D–A distance optimized by DFT calculations, R_D (R_A) is the radius of the electron donor (acceptor), ε_{REF} the static dielectric constant of the solvent used for the electrochemical studies, and ε_0 is the permittivity of free space.

The values of ΔG_{CS} indicated that the PET is thermodynamically allowed for all compounds listed in Table 4, and the driving forces for PET were larger in polar solvents (such as acetonitrile) than in nonpolar solvents (such as toluene), which corresponds to the fluorescence changes.

Table 4. Charge Separation Free Energy (ΔG_{CS}) [a] and Charge Separation Energy States (E_{CS}) for Compounds in Different Solvents

	ΔG_{CS} (eV)			E_{CS} (eV)		
	Toluene	DCM	ACN	Toluene	DCM	ACN
PTZ(2)-C-9An [b]	–0.16	–0.44	–0.51	2.94	2.66	2.59
PTZ-N-9An [c]	–0.49	–0.67	–0.75	2.66	2.48	2.43
DPA-9An [d]	–0.28	–0.39	–0.46	2.90	2.79	2.51
PTZ-N-2An [e]	–0.35	–0.60	–0.71	2.83	2.58	2.51

[a] The redox potentials are approximated based on the redox potential measured in acetonitrile. [b] E_{00} = 3.10 eV. [c] E_{00} = 3.19 eV. [d] E_{00} = 3.21 eV. [e] E_{00} = 3.22 eV.

3.4. Nanosecond Transient Absorption Spectroscopy: Study of the Triplet Excited State of the Dyads. To study the triplet excited states of the compact electron donor/acceptor dyads, nanosecond transient absorption spectra of the compounds were investigated (Figure 4). Upon pulsed laser excitation, a prominent excited-state absorption (ESA) band was observed at 430 nm for **An** (Figure 4a), which is the typical absorption of the T_1 state of anthracene ($T_1 \rightarrow T_n$ transitions).[83] The triplet state lifetime under the experimental conditions was determined as 123 μs. The efficient ISC of **An** (triplet state quantum yield Φ_T = 37% in toluene, Table 2) is attributed to the closely-lying S_1/T_2 states.[83–86] High singlet oxygen quantum yields (Φ_Δ = 70% in acetonitrile) were observed for **An** (Table 2).

Interestingly, we also observed high $^1O_2$ quantum yields for the PTZ–An dyads (Table 2). For instance, both **PTZ(2)-C-9An** and **PTZ-N-9An** show Φ_Δ up to 60%. In comparison, **DPA-9An**

shows less efficient ISC with a quantum yield lower than those of **An** and other dyads studied. Therefore, we assume that ISC upon photoexcitation is significant for the PTZ–An dyads.

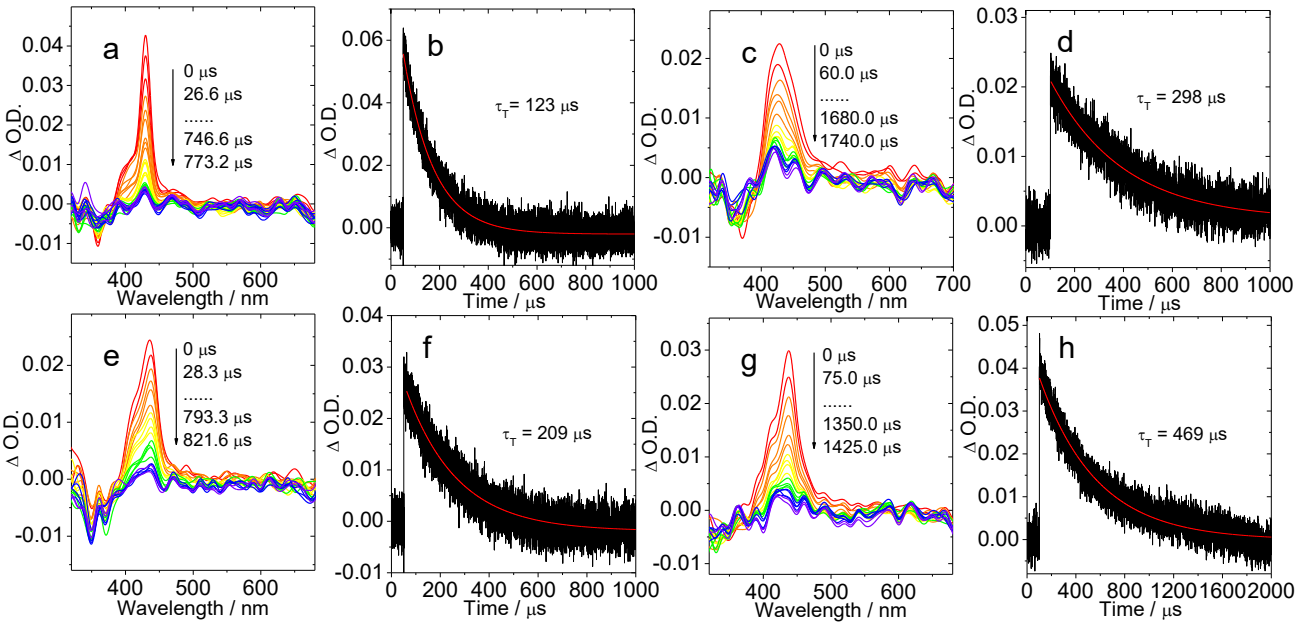

Figure 4. Nanosecond time-resolved transient absorption spectra of (a) **An** (λ_{ex} = 358 nm), (c) **PTZ(2)-C-9An** (λ_{ex} = 368 nm), (e) **PTZ-N-9An** (λ_{ex} = 368 nm), (g) **PTZ-N-2An** (λ_{ex} = 358 nm). Decay curves of (b) **An** (at 430 nm), (d) **PTZ(2)-C-9An** (at 440 nm), (f) **PTZ-N-9An** (at 440 nm), (h) **PTZ-N-2An** (at 440 nm) after pulsed laser excitation. The estimated error for the determination of the triplet state lifetime is ±5 μs. $c = 1.0 \times 10^{-5}$ M in degassed toluene at 20°C.

For all the PTZ–An dyads, a significant ESA band at 430 nm was observed upon photoexcitation (Figure 4), which is similar to that of anthracene (Figure 4a). Thus, the triplet state of PTZ–An dyads is localized on the anthracene moiety and does not show any charge transfer state (^{3}CT state) character. Our DFT computations support these notions (see below). The triplet-state lifetime of **PTZ-N-9An** was determined as 209 μs (the estimated error for the determination is ±5 μs) (Figure 4f).

The triplet quantum yields of **PTZ-N-9An** (34%) and **PTZ(2)-C-9An** (32%) are slightly lower than that of the previously reported DMJ–An dyads (Φ_{ISC} = 45%).[37] In the latter, the SOCT-ISC was achieved by rotation restriction via inducing *ortho*-methyl groups to the C–C single-bond linker. For PTZ–An dyads, however, the bulky PTZ itself exerts steric hindrance to the rotation.

For anthracene, the ESA band at 430 nm can be assigned to a $T_1 \rightarrow T_3$ transition. It is known that the T_1 state energy level of anthracene is 1.84 eV. The T_2 state (3.23 eV) is close to the S_1 state (ca. 3.28 eV, based on the fluorescence emission data). However, the higher excited states T_3 and T_4 lie 4.7 eV and 4.8 ~ 4.9 eV above the ground state, respectively.[84]

The fluorescence quantum yields of PTZ–An dyads (Φ_F < 8%) are substantially quenched as compared to that of anthracene (Φ_F = 33%. Table 2), but the singlet-oxygen quantum yield (Φ_Δ) does not decrease. We propose that SOCT-ISC plays a significant role, otherwise there will be a competition between $S_1 \rightarrow T_2$ and the CT process which will reduce Φ_Δ.

3.5. Femtosecond Transient Absorption Spectra. The ultrafast dynamics of the PTZ–An dyads has been analysed by applying pump-probe spectroscopy with sub-ps time resolution (Figure 5). The aim of these studies was the determination of the time constants for charge separation and triplet-state formation. All samples were excited at 390 nm, and the measurements were performed with DCM and toluene solutions of the compounds. The acquired kinetic traces were analysed by global fitting, using a sequential decay scheme with increasing lifetimes.

Evolution Associated Decay Spectra (EADS) obtained from the analysis of the transient absorption data of both **PTZ-N-9An** (Figure 5a) and **PTZ-N-2An** (Figure 5c) dyads, measured in DCM (spectra in toluene are provided in Supporting Information, Figure S16), are presented in Figure 5. Several spectral features are common to both systems. Soon after excitation, a broad

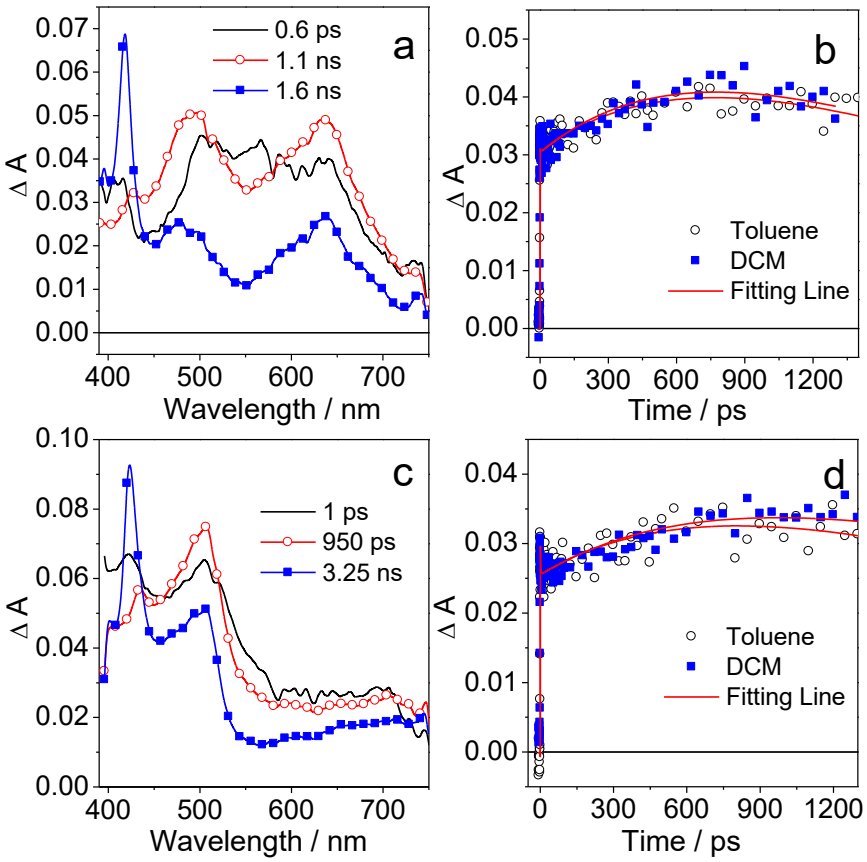

Figure 5. EADS obtained by global analysis of transient absorption data recorded for (a) **PTZ-N-9An** and (c) **PTZ-N-2An** in DCM. Panels (b) and (d) show the kinetic traces observed at 410 nm in DCM and toluene for the two systems, respectively. λ_{ex} = 390 nm.

ESA band is observed for **PTZ-N-9An** (Figure 5a), which develops in less than 1 ps, giving rise to a more structured absorption band. In the second EADS of Figure 5a, two intense transient absorption bands were observed at about 500 nm and 650 nm besides a less intense peak at about 435 nm. Based on the previous reports, the 500 nm band can be assigned to the absorption of the phenothiazine cation (approx. 510 nm), while the assignment of the anthracene anion band is more controversial.[87–90] An absorption band around 650 nm has been previously assigned to

anthracene anion,[91] as well as a peak in the 435–450 nm region.[88,89] The 650 nm band is however also observed for the singlet excited state spectrum of anthracene, while the band at around 435–450 nm is in the same region to the absorption of the anthracene triplet state. In any case, the clear observation of the phenothiazine cation band at 500 nm indicates the charge separation in the dyad. Within about 1 ns the intensity of all these ESA bands decreases, while a new sharp absorption, closely reminding that of the anthracene triplet state, as observed also in the nano-microsecond regime (Figure 4), develops (Figure 5a). The triplet-state formation dynamics is unaffected by the solvent, as shown from the comparison of the kinetic traces reported in Figure 5b.

A similar dynamic evolution is observed for **PTZ-N-2An** (Figure 5c). In this compound the rise of the radical pair $PTZ^{+\bullet}$-$An^{-\bullet}$ signals occurs with an even faster kinetics, since the characteristic absorption band of the $PTZ^{+\bullet}$ cation radical is observed already in the initial EADS (at 1 ps), which is in agreement with the stronger electronic coupling estimated for these dyads, due to their minor steric hindrance. The band at 650 nm has reduced intensity in this case, and it is also observed again with relative weak intensity when the measurement is repeated for the reference compound, **DPA-9An**, where charge separation occurs from the DPA to the **An** moiety upon photoexcitation (see transient spectra in Supporting Information, Figure S17). A possible explanation for the weak 650 nm band in **PTZ-N-2An** and **DPA-9An** is that it represents an absorption feature of the **An** anion, which is enhanced when the donor molecule is perpendicular to the acceptor, which is the case for **PTZ-N-9An**. The formation of **An** triplet state is also observed in case of **PTZ-N-2An**, in about 950 ps (Figure 5c), but not in case of **DPA-9An,** where the charge separated state has a longer lifetime (see Supporting Information, Figure S18). For **DPA-9An**, the band at 670 nm can be assigned to diphenylamine radical cation,[92] while that

at 460 nm could be assigned to An radical anion, which shows some shifts due to the different substitutent moiety.[88] The triplet state of An was not observed on this time scale, which may due to the extended lifetime of charge-separated state.

3.6. Time-Resolved Electron Paramagnetic Resonance (TREPR) Studies. Since anthracene has intrinsic ISC capability, the ISC mechanisms of the dyads should be verifiable with TREPR.[93] ISC is spin-state selective, thus the population rates of the three electron-spin sublevels of a triplet state (T_X, T_Y, T_Z; in the absence of an external magnetic field) are different, which gives rise to a specific electron-spin polarization (ESP) pattern.[52,57,94–100] The energetic degeneracy of the three triplet sublevels at zero magnetic field is lifted by the dipolar interaction of the two spin-unpaired electron spins, which is typically quantized by the so-called zero-field splitting parameters *D* and *E*. Different ISC mechanisms, such as the normal spin-orbit coupling ISC (SO-ISC), RP-ISC (enhanced by the hyperfine coupling interaction, HFI) and the SOCT-ISC, usually give rise to different ESP patterns of the triplet state. TREPR is an important tool for studying triplet excited states, as well as the underlying ISC mechanisms.[29,30,37] Moreover, the method is also useful to discriminate among ^{3}LE states (locally excited state, such as localized on anthracene) and ^{3}CT states.[99] Previously, ^{3}CT state was observed for some compact electron donor/acceptor dyads.[101–103] Especially the ZFS parameters, *D* and *E*, will be different for the ^{3}LE and the ^{3}CT state of a specific molecule.

Using TREPR, **An** was studied in frozen matrix (toluene at 80 K) upon pulsed laser excitation (Figure 6, top curve). The spectral line shape reveals an (E, E, E, A, A, A) ESP pattern similar to the previously published results.[37] The zero-field spitting (ZFS) parameters extracted from spectral simulations are D = 76.5 mT and E = –8.65 mT. Following the convention, that the energy levels of the zero-field triplet states are ordered according to $T_X > T_Y > T_Z$, with $D > 0$ and

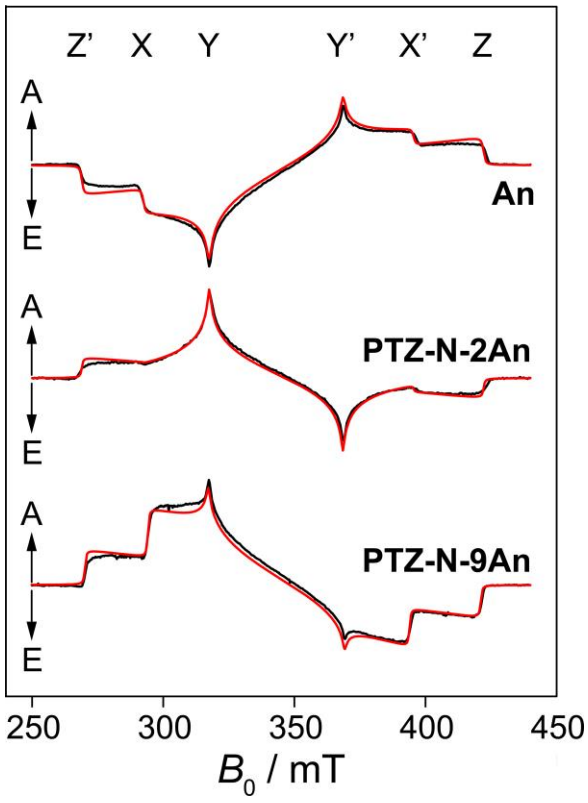

Figure 6. TREPR spectra of **An**, **PTZ-N-2An** and **PTZ-N-9An** in toluene recorded at 80 K and 300 ns after pulsed laser excitation (355 nm, ~10 ns, 1 mJ per pulse) defining time zero. The red curves are computer simulations of the experimental triplet-state TREPR spectra with the parameters given in Table 5. Positive signal amplitudes represent enhanced absorptive (A) and negative amplitudes emissive (E) polarization of the respective transition. All spectra were recorded at 9.687 GHz.

$E < 0$,[104] the following zero-field populations have been determined from least-squares fittings of the simulated spectrum to the experimental one: $A_X : A_Y : A_Z = 0.414 : 0.486 : 0.100$ (The set of populations is normalized according to $A_X + A_Y + A_Z = 1$). These data are in good agreement with the values published by Dance *et al.*, confirming that mostly T_X and T_Y are populated, with very

little population of T_Z.[37] Hence, SO-ISC is the dominant mechanism for generation of the zero-field triplet state with its sublevels.

Table 5. Zero-Field Splitting Parameters (*D* and *E*) and Relative Population Rates $A_{X,Y,Z}$ of the Zero-Field Spin States Obtained from Spectral Simulations of the Triplet-State TREPR Spectra of An and the Dyads PTZ-N-2An and PTZ-N-9An in a Toluene Matrix at 80 K [a]

molecule	*D* /mT	*E* /mT	A_X	A_Y	A_Z
An	76.52	–8.65	0.414	0.486	0.100
PTZ-N-2An	76.56	–8.67	0.359	0.066	0.575
PTZ-N-9An	75.41	–7.95	0.135	0.204	0.661

[a] All zero-field populations are normalized according to $A_X + A_Y + A_Z = 1$.

The two dyads, **PTZ-N-2An** and **PTZ-N-9An**, were also studied by TREPR (Figure 6, lower curves). The zero-field splitting parameters *D* and *E* extracted from spectral simulations are only marginally different from the ones of **An** but clearly different from those of the isolated PTZ unit, which has D = 131.4 mT and E = (–)15.2 mT.[105] This is a clear evidence, that the triplet state observed by TREPR is largely localized on the **An** unit, and it is not a ^{3}CT state, otherwise the $|D|$ value should be significantly smaller.[37]

Interestingly, the ESP patterns of the dyads are drastically different from that of **An**, thus indicating that the ISC mechanism is strongly affected by attachment to PTZ. For instance, the ESP pattern of **PTZ-N-9An** is (A, A, A, E, E, E); the thus over-populated magnetic sublevel of the triplet state is clearly T_Z, opposite to that of **An**. Furthermore, this pattern does not coincide with that expected for a radical-pair ISC mechanism (RP-ISC), which yields a (A, E, E, A, A, E) pattern, due to the population of the high-field triplet level T_0.[32] The observation of the CT

absorption and the CT fluorescence emission bands indicated that the electronic coupling between the electron donor and acceptor in the compact dyads is quite strong (Table 1 and Table 2), thus the electron exchange must be large, since $2J \propto V_{DA}^2$, hence, RP-ISC is unlikely.

Interestingly, we note that the ESP pattern of **PTZ-N-9An,** (A, A, A, E, E, E), is also different from the previously reported anthracene–julolidine compact dyads, which has an ESP pattern of (E, A, E, A, E, A).[37] Both dyads are consistent with SOCT-ISC, and the molecular structure profiles are literally the same. Our results indicate that even if the compact anthracene–electron-donor dyads have very similar conformation, the ESP phase, thus the spin selectivity of the ISC, may be different. Thus, not only the molecular conformation but also the structure of the electron donor/acceptor units influence the ESP pattern. This result is different from the previous conclusion that the ESP pattern solely depends on the molecular conformation.[37,52] Herein we demonstrate the ESP is also dependent on the electron donor/acceptor unit structure, this is a novel finding for the SOCT-ISC.

PTZ-N-2An has a structural feature different from that of **PTZ-N-9An**, although in both molecules the PTZ and An moieties are orthogonal to each other. The TREPR spectrum of the triplet state of **PTZ-N-2An** was also recorded (Figure 6). Interestingly, the ESP phase (A, A, A, E, E, E) is similar to that of **PTZ-N-9An**, however, the spectral shape is different. Based on our spectral simulations, we conclude that again T_Z is overpopulated, together with T_X. Its $|D|$ value (76.56 mT) is similar to that of **An** (76.52 mT) and **PTZ-N-9An** (75.41 mT). Thus we conclude that the triplet state for **PTZ-N-2An** is also localized on the anthracene unit, and it is not a ^{3}CT state. Similar effects of the topological feature of the compact electron donor/acceptor dyads were observed for naphthalene–acridine dyads.[52] It is clear that 'orthogonal' is not sufficient to describe the relation between the molecular geometry and the ESP pattern of the triplet state of

the electron donor/acceptor dyads. The ESP of the triplet state of the dyads is unlikely due to the transfer of electron spin polarization from the PTZ, although PTZ is known to undergo ISC.[106] ISC within the PTZ moiety is completed within ca. 1 ns.[106] This is much slower than photo-induced CS of the dyads (a few ps, Figure 5).

The time-profiles of the ESP signals after laser pulse were recorded (Supporting Information, Figure S19) and showed a mono-exponential decay function. The fitted time constants are 2.08 ± 0.01 μs, 1.50 ± 0.01 μs and 1.97 ± 0.01 μs for **An**, **PTZ-N-2An** and **PTZ-N-9An**, respectively. The time constants of approximately 2 μs are due to the spin-lattice relaxation of the electron-spin polarized population of the spin states at zero field, and consequently also at high field, to the Boltzmann thermal equilibrium at 80 K. The decay kinetics were different from the triplet-state lifetime of the compounds which were monitored with nanosecond transient absorption spectroscopy (123 μs for **An**. Figure 5b). There are some slight oscillations at early time after the laser pulse at $\tau = 0$ for **An** and **PTZ-N-2An**, which can be attributed to the Torrey oscillations (or B_1 oscillations).

3.7. DFT Computations to Rationalize the Photophysical Properties. The ground-state geometries of the dyads were optimized with DFT method by using various exchange and correlation functionals in order to well reproduce the maximum absorption wavelengths (see computational details). In Figure 7, the optimized structures obtained at the B3LYP/6-31G* level of theory are reported. For **PTZ-N-9An**, the dihedral angle between the PTZ and the An moieties is 85°, very close to an orthogonal geometry. For both **PTZ(2)-C-9An** and **PTZ-N-2An**, the energy-minimized geometry gives a dihedral angle of 80°. **DPA-9An** has the smallest dihedral angle between the electron donor and the An moiety, 73°. The trend of the dihedral angles is in full agreement with the UV−Vis absorption and the fluorescence spectra, i.e., the coupling is the

weakest in **PTZ-N-9An**, and **DPA-9An** is the dyad with the strongest coupling. As a result, the most significant CT band was observed for **DPA-9An**, but a weak tailing CT band was observed for **PTZ-N-9An** (Figures 1 and 2).

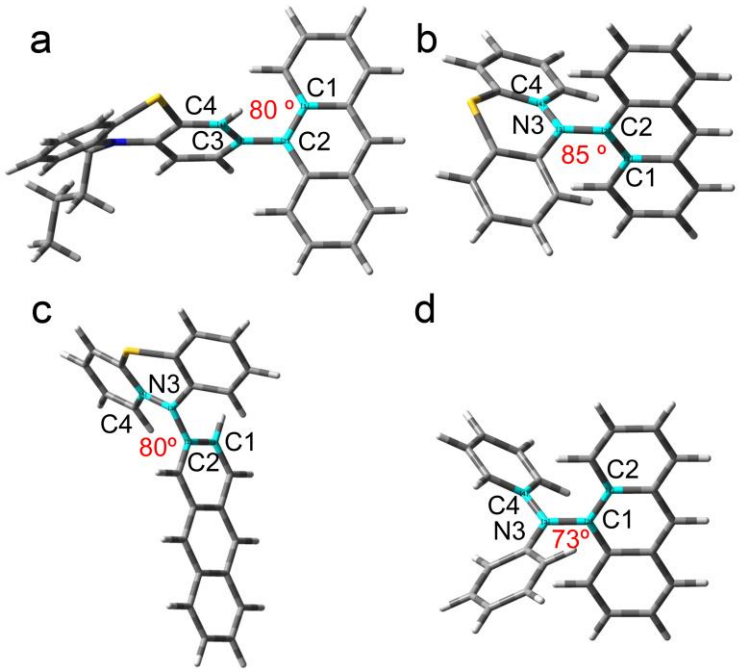

Figure 7. Optimized conformations of (a) **PTZ(2)-C-9An**, (b) **PTZ-N-9An**, (c) **PTZ-N-2An**, and (d) **DPA-9An** calculated by DFT at B3LYP/6−31G (d) level with Gaussian 09. Dihedral angle of phenothiazine and anthracene units are indicated in red.

In order to investigate the conformational constraints in the dyads in a more effective way, the potential energy curves of the rotation about the linker bonds were constructed (Figure 8). These potential energy curves do yield not only the energy minima, but also the steric hindrance about the rotation of the linkers, and the molecular conformations accessible at room temperature.

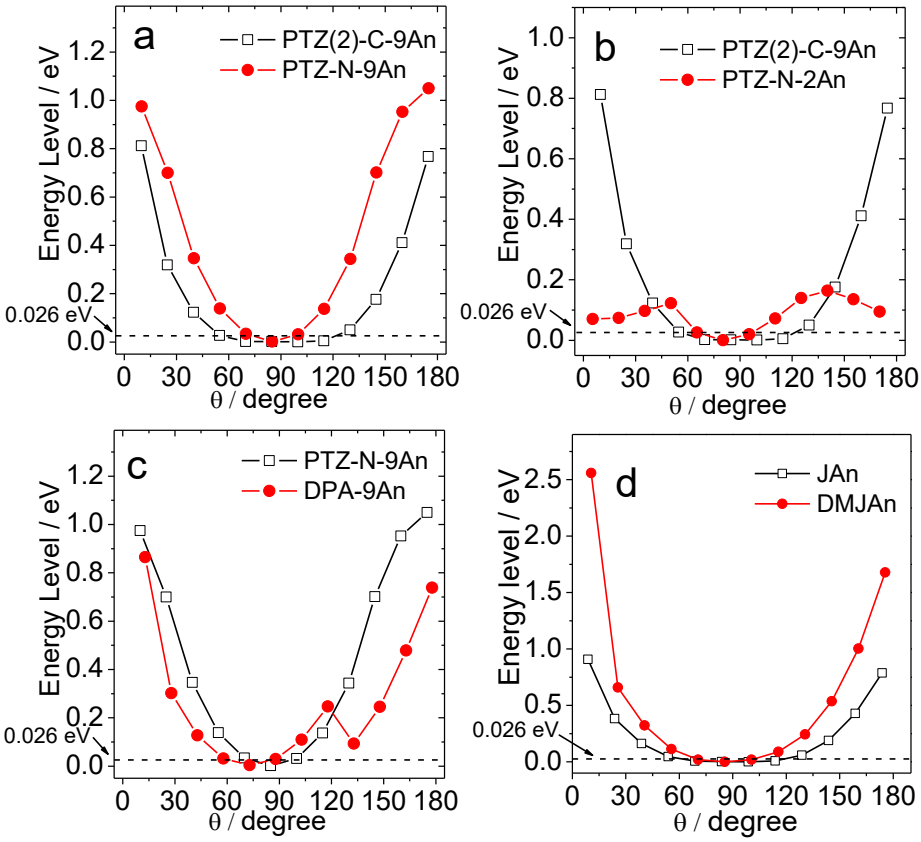

Figure 8. B3LYP/6–31G (d) calculated potential energy curves of the rotation around the linker bond of (a) **PTZ(2)-C-9An** and **PTZ-N-9An**, (b) **PTZ(2)-C-9An** and **PTZ-N-2An**, (c) **PTZ-N-9An** and **DPA-9An** (d) **J–An** and **DMJ–An** ground states. θ is the dihedral angle between phenothiazine or julolidine moiety and anthracene.

For **PTZ-N-9An**, the energy minimum is a conformation with a dihedral angle of 85°. The rotation about the C–N bond will experience significant encumbrance if it deviates from orthogonal geometry, and the energy increases sharply. At room temperature, the thermal energy (k_BT = 0.026 eV) is sufficient to populate the conformations with a dihedral angle in the range 73° ~ 97°.[48] For **PTZ(2)-C-9An**, the potential energy curve is more shallow; at room temperature the accessible conformations are those characterized by a dihedral angle ranging from 56° to 120°.

For **PTZ-N-2An**, the potential energy curve is drastically different from that of **PTZ(2)-C-9An** and **PTZ-N-9An**. No significant increase of the potential energy was observed upon rotation around the linker bond. However, the conformations accessible with the thermal energy k_BT is limited (from 75° to 95°).

The previously reported julolidine–An dyad was also studied (Figure 8d).[37] Without the methyl substituents the potential energy curve is flat and a vast number of conformations are accessible at k_BT (61° ~ 120°). By introducing methyl groups on the julolidine moiety, the conformation is restricted to a smaller range (between 69° ~ 102°). Thus, our approach was verified to be efficient for conformational restriction, i.e., for SOCT-ISC purpose.

Based on the optimized ground-state geometry, the molecular orbitals were examined (Figure 9). In all compounds, the LUMO is always localized on An moiety. For **PTZ-N-9An** and **PTZ-N-2An**, the dyad with the weaker electron coupling between the electron donor and acceptor, the HOMO and LUMO are localized on PTZ and An moieties, respectively. For **PTZ(2)-C-9An** with larger electronic couplings, the HOMO is more delocalized. This trend is clearer for **DPA-9An**, since the HOMO is highly delocalized, indicating strong coupling between the electron donor and the acceptors, which is in agreement with the UV–Vis absorption and fluorescence studies, as well as the V_{DA} values. The detailed transitions are reported in Table 6.

The simulated absorption spectra confirm what was experimentally found for **DPA-9An** and **PTZ(2)-C-9An**, evidencing that the CT band is observed. This is not the case for **PTZ-N-2An** and **PTZ-N-9An**, since the quite weak CT absorption band can be found in optical spectrum, even the associated oscillator strength is 0.

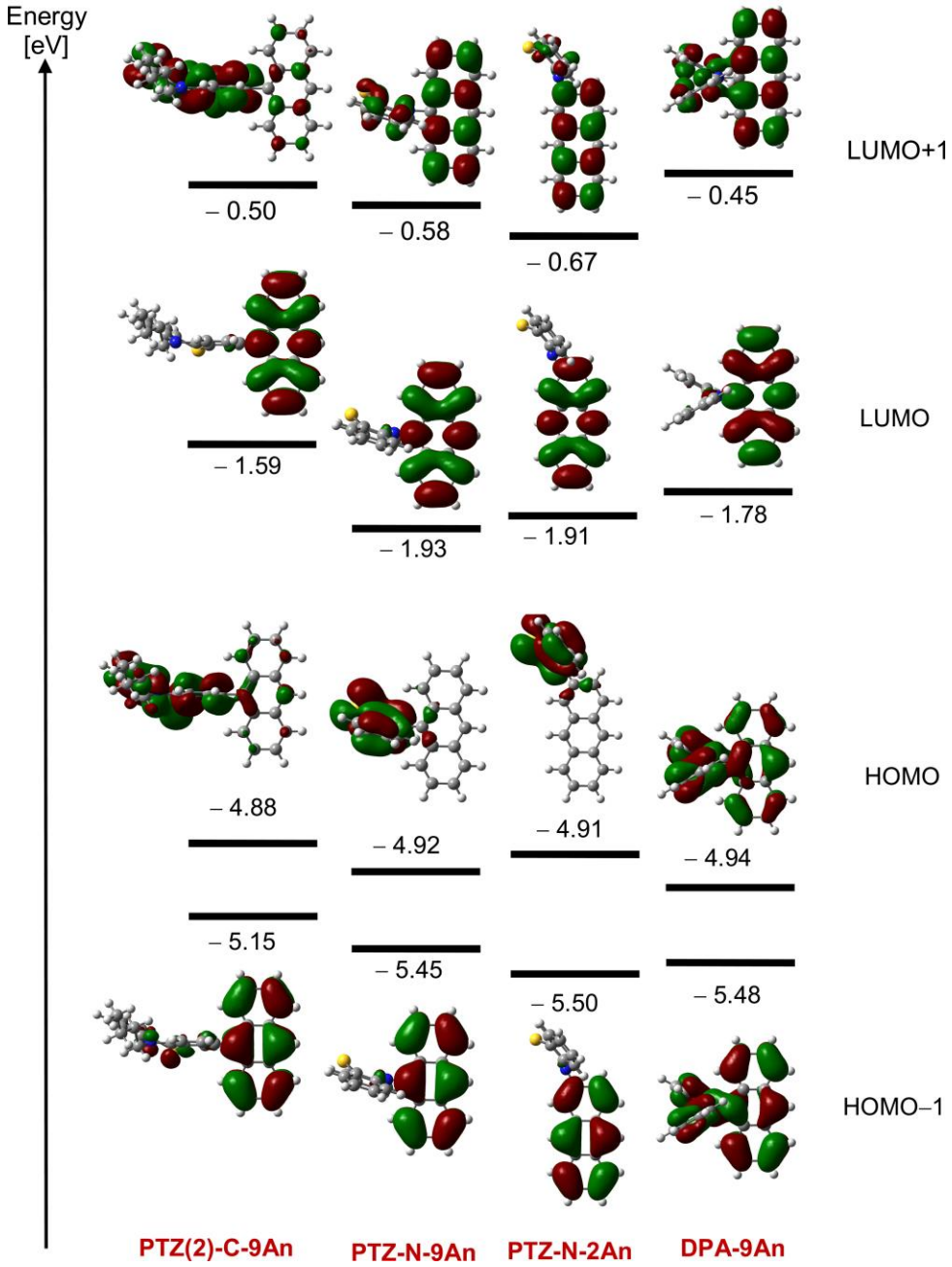

Figure 9. Energy Diagram and plot of the Four Goutermans' orbitals of **PTZ(2)-C-9An**, **PTZ-N-9An**, **PTZ-N-2An** and **DPA-9An** calculated at DFT (B3LYP/ 6–31G(d)) level with Gaussian 09W.

Table 6. Vertical Excitation Energies (ΔE in eV), Wavelength (λ in nm), and Oscillator Strengths *f* of the compounds Calculated by IEFPCM (TD–PBE0/6–31G) in Toluene [a]**

Compound	Excited State	MO contribution	Character	ΔE	ΔE^{adiab}	λ	f
PTZ(2)–C–9An	S_1	H → L (99%)	^{1}CT	2.95	2.64	421	0.125
	S_2	H–1 → L (98%)	^{1}LE$_a$	3.30	3.04	375	0.118
	T_1	H–1 → L (75%)	^{3}LE$_a$	1.63			
	T_2	H → L+1 (56%)	^{3}CT	2.81			
	T_3	H → L (60%)	^{3}LE$_p$	3.02			
	T_4	H–4 → L (37%),	^{3}LE$_a$	3.22			
PTZ–N–9An	S_1	H→ L (99%)	^{1}CT	2.53	2.85	490	0.000
	S_2	H–1 → L (99%)	^{1}LE$_a$	3.24	3.74	383	0.156
	T_1	H–1 → L (98%)	^{3}LE$_a$	1.62			
	T_2	H → L (98%)	^{3}CT	2.52			
	T_3	H → L+2 (44%),	^{3}LE$_p$	2.92			
	T_4	H–4 → L (30%),	^{3}LE$_a$	3.17			
PTZ–N–2An	S_1	H → L (98%)	^{1}CT	2.77	2.29	447	0.000
	S_2	H–1 → L (99%)	^{1}LE$_a$	3.32	3.08	373	0.083
	T_1	H–1 → L (97%)	^{3}LE$_a$	1.69			
	T_2	H → L (96%)	^{3}CT	2.75			
	T_3	H → L+2 (57%)	^{3}LE$_p$	2.98			
	T_4	H–4 → L (41%),	^{3}LE$_a$	3.24			
DPA–9An	S_1	H → L (95%)	^{1}CT	2.70	2.52	459	0.090
	S_2	H–1 → L (94%)	^{1}LE$_a$	3.36	3.10	369	0.079
	T_1	H → L (58%),	^{3}LE$_a$	1.58			
	T_2	H–1 → L (55%),	^{3}CT	2.78			
	T_3	H → L+2 (41%),	^{3}LE$_p$	3.14			
	T_4	H–6 → L (29%),	^{3}LE$_a$	3.20			

[a] ΔE^{adiab} energies (in eV) are obtained from the relaxed structures of excited states.

The EDDMs reported in Figure 10 for **PTZ-N-9An** and **DPA-9An** clearly show that both S_1 and T_2 states are characterized by an intramolecular charge-transfer from the PTZ or the DPA to the An unit, while all the other examined excited states are An (S_2, T_1 and T_4) or PTZ/DPA localized (T_3).

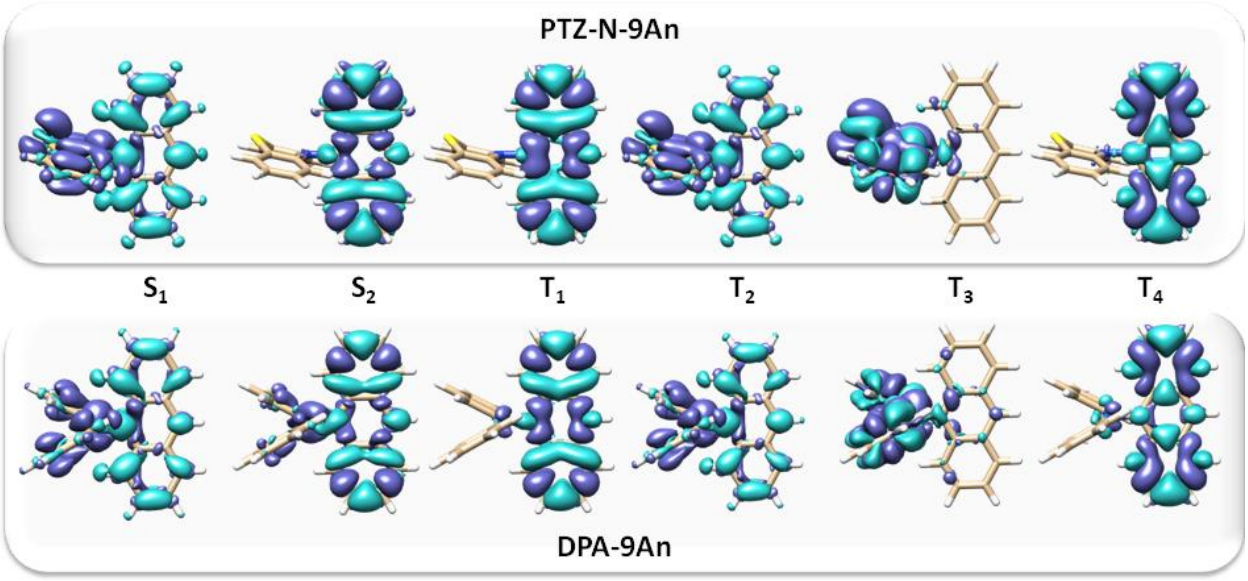

Figure 10. Electron density difference maps for **PTZ-N-9An** and **DPA-9An** computed between low-lying singlet and triplet excited states; the light blue or violet regions indicating increase or decrease in the electronic density upon electronic transition, respectively.

The different character of the excited states can give an indication of which state can be involved in an efficient ISC, since, according to the El-Sayed rules, the rate of ISC is larger if the radiationless transition involves a change of molecular orbital type. Accordingly, the increasing of spin-orbit coupling between singlet and triplet states may lead to more efficient ISC.

For all compounds, the spin-orbit matrix elements between S_1 and T_1 are larger than that between the S_1 and T_2 states (Table 7), which indicates that the $S_1 \rightarrow T_1$ ISC is more efficient

than $S_1 \rightarrow T_2$. For PTZ–An compounds, the S_1 state is a charge transfer state and the T_1 state is the LE triplet state.

Table 7. Spin-Orbit Matrix Elements (SOC), Vertical Energy Gaps (ΔE) between the Plausible States [a]

Compound	electronic transition	SOC (cm^{-1})	ΔE (eV)
PTZ(2)-C-9An	$S_1 \rightarrow T_1$	2.37	1.29
	$S_1 \rightarrow T_2$	0.74	0.87
	$S_2 \rightarrow T_1$	1.30	1.51
	$S_2 \rightarrow T_2$	1.83	1.09
	$S_2 \rightarrow T_3$	0.92	0.09
PTZ-N-9An	$S_1 \rightarrow T_1$	0.37	0.91
	$S_1 \rightarrow T_2$	0.00	0.01
	$S_2 \rightarrow T_1$	0.00	1.61
	$S_2 \rightarrow T_2$	0.32	0.71
	$S_2 \rightarrow T_3$	0.03	0.32
PTZ-N-2An	$S_1 \rightarrow T_1$	0.35	1.08
	$S_1 \rightarrow T_2$	0.05	0.02
	$S_2 \rightarrow T_1$	0.05	1.63
	$S_2 \rightarrow T_2$	0.23	0.57
	$S_2 \rightarrow T_3$	0.02	0.34
DPA-9An	$S_1 \rightarrow T_1$	0.58	1.12
	$S_1 \rightarrow T_2$	0.00	–0.08
	$S_2 \rightarrow T_1$	0.61	1.78
	$S_2 \rightarrow T_2$	0.66	0.58
	$S_2 \rightarrow T_3$	0.35	0.22

[a] The first singlet excited state optimized structure and by using QR-TDB3LYP/cc-pVDZ.

These are in accordance with the results of femtosecond transition spectra, suggesting the ISC in PTZ–An compounds are $PTZ^{+\bullet}–An^{-\bullet} \rightarrow PTZ–^{3*}An$. Therefore, the only possible pathway that

leads to the triplet state population should entail the coupling between S_1 and T_1. In the case of **PTZ-N-9An** and **PTZ-N-2An** compounds, an internal conversion (CS) is required to occur before the SOCT process in order to populate the low-lying singlet state with CT character.

Scheme 2. Energy Diagram of the Photophysical Processes of the Compounds (a) An, (b) PTZ-N-2An, (c) PTZ(2)-C-9An [a]

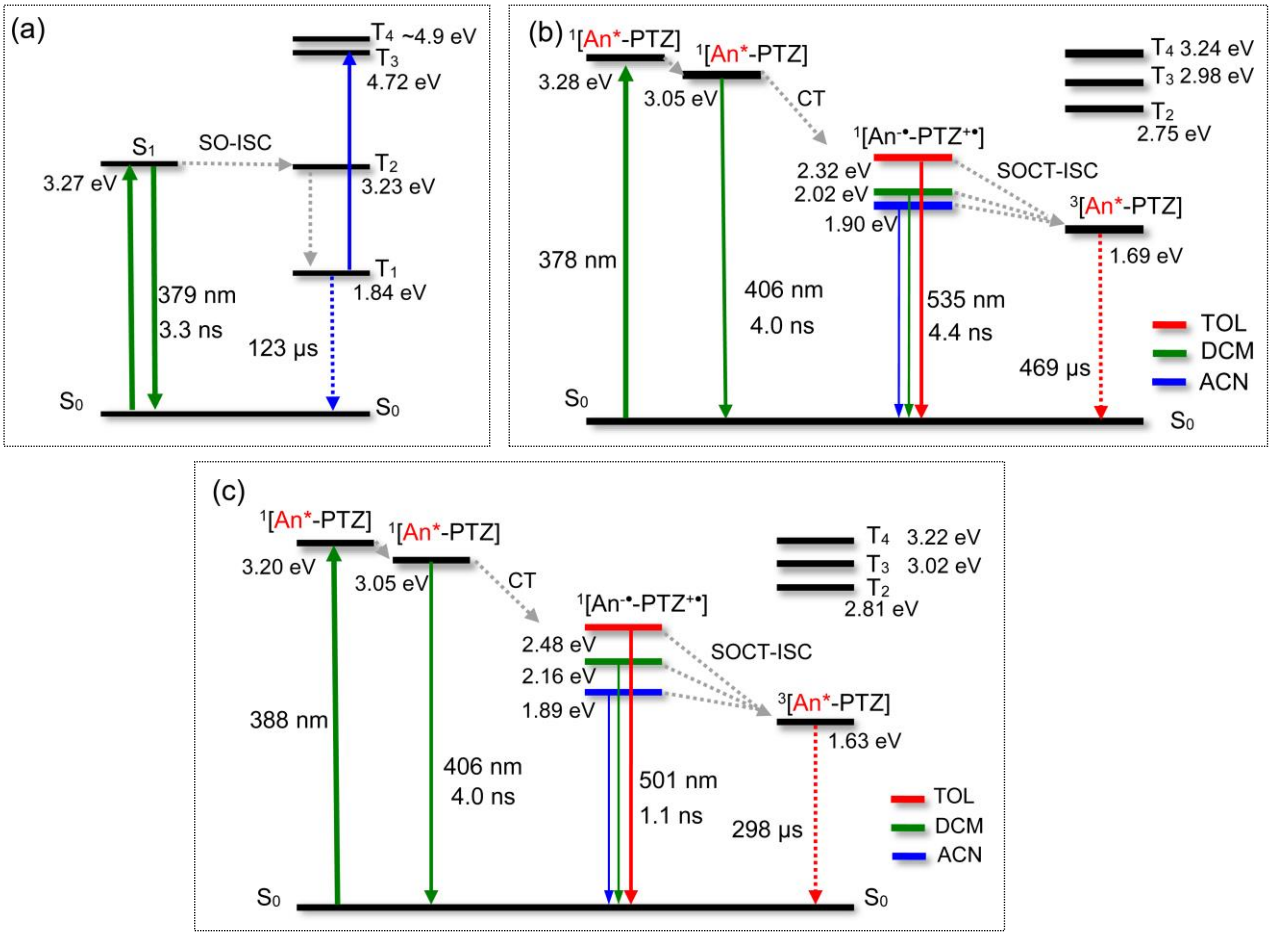

[a] The energy levels of the excited singlet states are derived from the spectroscopic data, the energy level of charge transfer states are obtained from the CT emission band, and the energy levels of the triplet states are from IEFPCM calculation at (TD-PBE0/6-31G**) level with Gaussian 09W (in toluene). The transition of $T_1 \rightarrow T_n$ is from the nanosecond transient absorption data and IEFPCM computations.

The photophysical properties of the compounds are summarized in Scheme 2. For **An**, the ISC is via $S_1 \rightarrow T_2$, as the two states share the same energy level, then followed by $T_2 \rightarrow T_1$. For

PTZ–An dyads, the S_1 state (^{1}CT state) energy level is lower than the T_2 state. However, the ^{1}CT state energy level is close to the low-lying T_1 state energy level, thus, only the $^1CT \rightarrow T_1$ ISC is possible. Considering the molecular orbital angular momentum changes during the charge recombination (CR), the ISC can be enhanced, with the so-called SOCT-ISC mechanism. Accordingly, efficient ISC was observed, even with relatively large S_1/T_1 state energy gap.

4. CONCLUSIONS

Phenothiazine (PTZ)–Anthracene (An) compact electron donor/acceptor dyads were prepared to study the spin-orbit charge-transfer induced intersystem crossing (SOCT-ISC). To achieve efficient SOCT-ISC, the electron donor (PTZ) and the acceptor (An) should adopt an orthogonal conformation. The molecular conformation was systematically varied by rotation restriction, exerted by steric hindrance. The intensities of the electronic coupling between the electron donor and acceptor were quantified with the matrix elements (V_{DA}). Charge transfer (CT) absorption and fluorescence bands were observed for the dyads, for which the intensities varied according to the different V_{DA} values. The fluorescence of the anthryl moiety was significantly quenched in the dyads, and efficient ISC was confirmed with nanosecond transient absorption spectroscopy (Φ_Δ = 65%, τ_T = 209 μs). Using femtosecond transient absorption spectroscopy, photo-induced charge separation (<1 ps) and recombination (950 ps) was revealed. Time-resolved electron paramagnetic resonance (TREPR) spectra reveal the electron spin polarization (ESP) patterns of the triplet state of the dyads, (A, A, A, E, E, E), which are drastically different from that of pristine anthracene, (E, E, E, A, A, A), thus confirming SOCT-ISC. The ESP patterns of the dyads highly depend on the topological features of the compounds, and the assumption of an orthogonal geometry is not sufficient to describe the relationship between the molecular conformation and the specific ESP pattern observed for the different systems. We further

confirmed that the ESP pattern of the triplet state not only depends on the molecular geometry, but also on the structure of the electron donor. The rotation steric hindrance was analyzed with the potential energy curves and PTZ was found to be an ideal electron donor to induce rotation steric hindrance about the linker, thus to attain SOCT-ISC, due to its puckered structure. Theoretical computations show that spin-orbit coupling (SOC) between the S_1 and T_1 state (up to 2.37 cm^{-1}) is larger than the S_1/T_2 coupling (<1 cm^{-1}). These new findings are useful for the design of novel molecular systems to control the fate of the charge recombination, a ubiquitous process in a wide variety of organic functional materials and devices.

ASSOCIATED CONTENT

Supporting Information

General experimental methods, ^{1}H, ^{13}C NMR data and HRMS spectra of the compounds and the theoretical computation details. This material is available free of charge via the internet at http://pubs.acs.org.

AUTHOR INFORMATION

Corresponding Authors

*E-mail: zhaojzh@dlut.edu.cn

*E-mail: didonato@lens.unifi.it

*E-mail: gloria.mazzone@unical.it

*E-mail: stefan.weber@physchem.uni-freiburg.de

Notes

The authors declare no competing financial interest.

ACKNOWLEDGEMENT

J. Z thanks the NSFC (214730202, 21673031, 21761142005, 21273028, 21603021, 21576043 and 21421005), the Fundamental Research Funds for the Central Universities (DUT16TD25, DUT15ZD224, DUT2016TB12) for financial support. G. M and N. R. gratefully acknowledge the Università della Calabria for financial support. S. W. and T. B. thank Sabine Richert (University of Freiburg) for fruitful discussions.

REFERENCES

(1) de Silva, A. P.; Gunaratne, H. N.; Gunnlaugsson, T.; Huxley, A. J.; McCoy, C. P.; Rademacher, J. T.; Rice, T. E. Signaling Recognition Events with Fluorescent Sensors and Switches. *Chem. Rev.* **1997**, *97*, 1515–1566.

(2) Shi, L.; Xia, W. Photoredox Functionalization of C–H Bonds Adjacent to a Nitrogen Atom. *Chem. Soc. Rev.* **2012**, *41*, 7687–7697.

(3) Wu, Y.; Zhu, W. Organic Sensitizers from D–π–A to D–A–π–A: Effect of the Internal Electron-Withdrawing Units on Molecular Absorption, Energy Levels and Photovoltaic Performances. *Chem. Soc. Rev.* **2013**, *42*, 2039–2058.

(4) Hari, D. P.; König, B. The Photocatalyzed Meerwein Arylation: Classic Reaction of Aryl Diazonium Salts in a New Light. *Angew. Chem. Int. Ed.* **2013**, *52*, 4734–4743.

(5) Schäferling, M. The Art of Fluorescence Imaging with Chemical Sensors. *Angew. Chem. Int. Ed.* **2012**, *51*, 3532–3554.

(6) Xiang, H.; Zhou, L.; Feng, Y.; Cheng, J.; Wu, D.; Zhou, X. Tunable Fluorescent/Phosphorescent Platinum (II) Porphyrin–Fluorene Copolymers for Ratiometric Dual Emissive Oxygen Sensing. *Inorg. Chem.* **2012**, *51*, 5208–5212.

(7) Erbas-Cakmak, S.; Akkaya, E. U. Cascading of Molecular Logic Gates for Advanced Functions: A Self-Reporting, Activatable Photosensitizer. *Angew. Chem. Int. Ed.* **2013**, *52*, 11364–11368.

(8) Awuah, S. G.; You, Y. Boron Dipyrromethene (Bodipy)-Based Photosensitizers for Photodynamic Therapy. *RSC Adv.* **2012**, *2*, 11169–11183.

(9) Majumdar, P.; Nomula, R.; Zhao, J. Activatable Triplet Photosensitizers: Magic Bullets for Targeted Photodynamic Therapy. *J. Mater. Chem. C* **2014**, *2*, 5982–5997.

(10) Garci, A.; Mbakidi, J.-P.; Chaleix, V.; Sol, V.; Orhan, E.; Therrien, B. Tunable Arene Ruthenium Metallaprisms to Transport, Shield, and Release Porphin in Cancer Cells. *Organometallics*. **2015**, *34*, 4138–4146.

(11) Singh-Rachford, T. N.; Castellano, F. N. Photon Upconversion Based on Sensitized Triplet–Triplet Annihilation. *Coordin. Chem. Rev.* **2010**, *254*, 2560–2573.

(12) Zhao, J.; Ji, S.; Guo, H. Triplet–Triplet Annihilation Based Upconversion: From Triplet Sensitizers and Triplet Acceptors to Upconversion Quantum Yields. *RSC Adv.* **2011**, *1*, 937–950.

(13) Simon, Y. C.; Weder, C. Low-Power Photon Upconversion through Triplet–Triplet Annihilation in Polymers. *J. Mater. Chem.* **2012**, *22*, 20817–20830.

(14) Xun, Z.; Zeng, Y.; Chen, J.; Yu, T.; Zhang, X.; Yang, G.; Li, Y. Pd–Porphyrin Oligomers Sensitized for Green-to-Blue Photon Upconversion: The More the Better? *Chem.–Eur. J.* **2016**, *22*, 8654–8662.

(15) Yanai, N.; Kimizuka, N. New Triplet Sensitization Routes for Photon Upconversion: Thermally Activated Delayed Fluorescence Molecules, Inorganic Nanocrystals, and Singlet-to-Triplet Absorption. *Acc. Chem. Res.* **2017**, *50*, 2487–2495.

(16) Loudet, A.; Burgess, K. Bodipy Dyes and Their Derivatives: Syntheses and Spectroscopic Properties. *Chem. Rev.* **2007**, *107*, 4891–4932.

(17) Ulrich, G.; Ziessel, R.; Harriman, A. The Chemistry of Fluorescent Bodipy Dyes: Versatility Unsurpassed. *Angew. Chem. Int. Ed.* **2008**, *47*, 1184–1201.

(18) Lu, H.; Mack, J.; Yang, Y.; Shen, Z. Structural Modification Strategies for the Rational Design of Red/NIR Region Bodipys. *Chem. Soc. Rev.* **2014**, *43*, 4778–4823.

(19) Ziessel, R.; Harriman, A. Artificial Light-Harvesting Antennae: Electronic Energy Transfer by Way of Molecular Funnels. *Chem. Commun.* **2011**, *47*, 611–631.

(20) Fan, J.; Hu, M.; Zhan, P.; Peng, X. Energy Transfer Cassettes Based on Organic Fluorophores: Construction and Applications in Ratiometric Sensing. *Chem. Soc. Rev.* **2013**, *42*, 29–43.

(21) Hashimoto, H.; Sugai, Y.; Uragami, C.; Gardiner, A. T.; Cogdell, R. J. Natural and Artificial Light-Harvesting Systems Utilizing the Functions of Carotenoids. *J. Photochem. Photobio. C* **2015**, *25*, 46–70.

(22) Verhoeven, J. W.; van Ramesdonk, H. J.; Groeneveld, M. M.; Benniston, A. C.; Harriman, A. Long-Lived Charge-Transfer States in Compact Donor–Acceptor Dyads. *ChemPhysChem* **2005**, *6*, 2251–2260.

(23) Verhoeven, J. W. On the Role of Spin Correlation in the Formation, Decay, and Detection of Long-Lived, Intramolecular Charge-Transfer States. *J. Photochem. Photobio. C* **2006**, *7*, 40–60.

(24) Ziessel, R.; Allen, B. D.; Rewinska, D. B.; Harriman, A. Selective Triplet-State Formation During Charge Recombination in a Fullerene/Bodipy Molecular Dyad (Bodipy= Borondipyrromethene). *Chem.–Eur. J.* **2009**, *15*, 7382–7393.

(25) Hankache, J.; Wenger, O. S. Large Increase of the Lifetime of a Charge-Separated State in a Molecular Triad Induced by Hydrogen-Bonding Solvent. *Chem.–Eur. J.* **2012**, *18*, 6443–6447.

(26) Kc, C. B.; Lim, G. N.; Nesterov, V. N.; Karr, P. A.; D'Souza, F. Phenothiazine–Bodipy–Fullerene Triads as Photosynthetic Reaction Center Models: Substitution and Solvent Polarity Effects on Photoinduced Charge Separation and Recombination. *Chem. –Eur. J.* **2014**, *20*, 17100–17112.

(27) Lee, S.-H.; Chan, C. T.-L.; Wong, K. M.-C.; Lam, W. H.; Kwok, W.-M.; Yam, V. W.-W. Design and Synthesis of Bipyridine Platinum (II) Bisalkynyl Fullerene Donor–Chromophore–Acceptor Triads with Ultrafast Charge Separation. *J. Am. Chem. Soc.* **2014**, *136*, 10041–10052.

(28) Collini, M. A.; Thomas, M. B.; Bandi, V.; Karr, P. A.; D'Souza, F. Directly Attached Bisdonor-BF_2 Chelated Azadipyrromethene-Fullerene Tetrads for Promoting Ground and Excited State Charge Transfer. *Chem. –Eur. J.* **2017**, *23*, 4450–4461.

(29) Weiss, E. A.; Ratner, M. A.; Wasielewski, M. R. Direct Measurement of Singlet−Triplet Splitting within Rodlike Photogenerated Radical Ion Pairs Using Magnetic Field Effects: Estimation of the Electronic Coupling for Charge Recombination. *J. Phys. Chem. A* **2003**, *107*, 3639–3647.

(30) Weiss, E. A.; Ahrens, M. J.; Sinks, L. E.; Gusev, A. V.; Ratner, M. A.; Wasielewski, M. R. Making a Molecular Wire: Charge and Spin Transport through *para*-Phenylene Oligomers. *J. Am. Chem. Soc.* **2004**, *126*, 5577–5584.

(31) Weiss, E. A.; Ahrens, M. J.; Sinks, L. E.; Ratner, M. A.; Wasielewski, M. R. Solvent Control of Spin-Dependent Charge Recombination Mechanisms within Donor–Conjugated Bridge−Acceptor Molecules. *J. Am. Chem. Soc.* **2004**, *126*, 9510–9511.

(32) Dance, Z. E. X.; Mi, Q.; McCamant, D. W.; Ahrens, M. J.; Ratner, M. A.; Wasielewski, M. R. Time-Resolved EPR Studies of Photogenerated Radical Ion Pairs Separated by *p*-Phenylene Oligomers and of Triplet States Resulting from Charge Recombination. *J. Phys. Chem. B* **2006**, *110*, 25163–25173.

(33) Suneesh, C. V.; Gopidas, K. R. Long-Lived Photoinduced Charge Separation Due to the Inverted Region Effect in 1,6-Bis(Phenylethynyl) Pyrene–Phenothiazine Dyad. *J. Phys. Chem. C* **2010**, *114*, 18725–18734.

(34) Hankache, J.; Wenger, O. S. Organic Mixed Valence. *Chem. Rev.* **2011**, *111*, 5138–5178.

(35) Heckmann, A.; Lambert, C. Organic Mixed-Valence Compounds: A Playground for Electrons and Holes. *Angew. Chem. Int. Ed.* **2012**, *51*, 326–392.

(36) Zhong, Y.-W.; Gong, Z.-L.; Shao, J.-Y.; Yao, J. Electronic Coupling in Cyclometalated Ruthenium Complexes. *Coord. Chem. Rev.* **2016**, *312*, 22–40.

(37) Dance, Z. E.; Mickley, S. M.; Wilson, T. M.; Ricks, A. B.; Scott, A. M.; Ratner, M. A.; Wasielewski, M. R. Intersystem Crossing Mediated by Photoinduced Intramolecular Charge Transfer: Julolidine−Anthracene Molecules with Perpendicular π Systems. *J. Phys. Chem. A* **2008**, *112*, 4194–4201.

(38) Benniston, A. C.; Harriman, A.; Whittle, V. L.; Zelzer, M.; Harrington, R. W.; Clegg, W. Exciplex-Like Emission from a Closely-Spaced, Orthogonally-Sited Anthracenyl-Boron Dipyrromethene (Bodipy) Molecular Dyad. *Photochem. Photobiol. Sci.* **2010**, *9*, 1009–1017.

(39) Sasaki, S.; Hattori, K.; Igawa, K.; Konishi, G.-i. Directional Control of π-Conjugation Enabled by Distortion of the Donor Plane in Diarylaminoanthracenes: A Photophysical Study. *J. Phys. Chem. A* **2015**, *119*, 4898–4906.

(40) Epelde-Elezcano, N.; Palao, E.; Manzano, H.; Prieto-Castañeda, A.; Agarrabeitia, A. R.; Tabero, A.; Villanueva, A.; de la Moya, S.; López-Arbeloa, Í.; Martínez-Martínez, V. Rational Design of Advanced Photosensitizers Based on Orthogonal Bodipy Dimers to Finely Modulate Singlet Oxygen Generation. *Chem.–Eur. J.* **2017**, *23*, 4837–4848.

(41) Zhang, X.-F.; Yang, X.; Xu, B. PET-Based Bisbodipy Photosensitizers for Highly Efficient Excited Triplet State and Singlet Oxygen Generation: Tuning Photosensitizing Ability by Dihedral Angles. *Phys. Chem. Chem. Phys.* **2017**, *19*, 24792–24804.

(42) Filatov, M. A.; Karuthedath, S.; Polestshuk, P. M.; Savoie, H.; Flanagan, K. J.; Sy, C.; Sitte, E.; Telitchko, M.; Laquai, F.; Boyle, R. W. Generation of Triplet Excited States Via

Photoinduced Electron Transfer in *meso*-Anthra-Bodipy: Fluorogenic Response toward Singlet Oxygen in Solution and in Vitro. *J. Am. Chem. Soc.* **2017**, *139*, 6282−6285.

(43) Tanaka, H.; Shizu, K.; Miyazaki, H.; Adachi, C. Efficient Green Thermally Activated Delayed Fluorescence (TADF) from a Phenoxazine–Triphenyltriazine (PXZ–TRZ) Derivative. *Chem. Commun.* **2012**, *48*, 11392−11394.

(44) Tao, Y.; Yuan, K.; Chen, T.; Xu, P.; Li, H.; Chen, R.; Zheng, C.; Zhang, L.; Huang, W. Thermally Activated Delayed Fluorescence Materials Towards the Breakthrough of Organoelectronics. *Adv. Mater.* **2014**, *26*, 7931−7958.

(45) Wong, M. Y.; Zysman-Colman, E. Purely Organic Thermally Activated Delayed Fluorescence Materials for Organic Light-Emitting Diodes. *Adv. Mater.* **2017**, *29*, 1605444.

(46) Penfold, T. J. On Predicting the Excited-State Properties of Thermally Activated Delayed Fluorescence Emitters. *J. Phys. Chem. C* **2015**, *119*, 13535−13544.

(47) Samanta, P. K.; Kim, D.; Coropceanu, V.; Brédas, J.-L. Up-Conversion Intersystem Crossing Rates in Organic Emitters for Thermally Activated Delayed Fluorescence: Impact of the Nature of Singlet vs Triplet Excited States. *J. Am. Chem. Soc.* **2017**, *139*, 4042−4051.

(48) Yao, L.; Pan, Y.; Tang, X.; Bai, Q.; Shen, F.; Li, F.; Lu, P.; Yang, B.; Ma, Y. Tailoring Excited-State Properties and Electroluminescence Performance of Donor–Acceptor Molecules through Tuning the Energy Level of the Charge-Transfer State. *J. Phys. Chem. C* **2015**, *119*, 17800−17808.

(49) Wiederrecht, G. P.; Svec, W. A.; Wasielewski, M. R.; Galili, T.; Levanon, H. Triplet States with Unusual Spin Polarization Resulting from Radical Ion Pair Recombination at Short Distances. *J. Am. Chem. Soc.* **1999**, *121*, 7726–7727.

(50) Bandi, V.; Gobeze, H. B.; Lakshmi, V.; Ravikanth, M.; D'Souza, F. Vectorial Charge Separation and Selective Triplet-State Formation During Charge Recombination in a Pyrrolyl-Bridged Bodipy–Fullerene Dyad. *J. Phys. Chem. C* **2015**, *119*, 8095–8102.

(51) Okada, T.; Karaki, I.; Matsuzawa, E.; Mataga, N.; Sakata, Y.; Misumi, S. Ultrafast Intersystem Crossing in Some Intramolecular Heteroexcimers. *J. Phys. Chem.* **1981**, *85*, 3957–3960.

(52) van Willigen, H.; Jones, G.; Farahat, M. S. Time-Resolved EPR Study of Photoexcited Triplet-State Formation in Electron-Donor-Substituted Acridinium Ions. *J. Phys. Chem.* **1996**, *100*, 3312–3316.

(53) Zhang, X.-F.; Feng, N. Photoinduced Electron Transfer-based Halogen-free Photosensitizers: Covalent *meso*-Aryl (Phenyl, Naphthyl, Anthryl, and Pyrenyl) as Electron Donors to Effectively Induce the Formation of the Excited Triplet State and Singlet Oxygen for BODIPY Compounds. *Chem. Asian J.* **2017**, *12*, 2447–2456.

(54) Wang, Z.; Zhao, J. Bodipy–Anthracene Dyads as Triplet Photosensitizers: Effect of Chromophore Orientation on Triplet-State Formation Efficiency and Application in Triplet–Triplet Annihilation Upconversion. *Org. Lett.* **2017**, *19*, 4492–4495.

(55) Chen, K.; Yang, W.; Wang, Z.; Iagatti, A.; Bussotti, L.; Foggi, P.; Ji, W.; Zhao, J.; Di Donato, M. Triplet Excited State of Bodipy Accessed by Charge Recombination and Its

Application in Triplet–Triplet Annihilation Upconversion. *J. Phys. Chem. A* **2017**, *121*, 7550–7564.

(56) Filatov, M. A.; Karuthedath, S.; Polestshuk, P. M.; Callaghan, S.; Flanagan, K. J.; Telitchko, M.; Wiesner, T.; Laquai, F.; Senge, M. O. Control of Triplet State Generation in Heavy Atom-Free Bodipy-Anthracene Dyads by Media Polarity and Structural Factors. *Phys. Chem. Chem. Phys*. **2018**, *20*, 8016–8031.

(57) Wiederrecht, G. P.; Svec, W. A.; Wasielewski, M. R.; Galili, T.; Levanon, H. Novel Mechanism for Triplet State Formation in Short Distance Covalently Linked Radical Ion Pairs. *J. Am. Chem. Soc.* **2000**, *122*, 9715–9722.

(58) Suzuki, Y.; Fukui, N.; Murakami, K.; Yorimitsu, H.; Osuka, A. Amination of meso-Bromoporphyrins and 9-Haloanthracenes with Diarylamines Catalyzed by a Palladium–PEPPSI Complex. *Asian J. Org. Chem.* **2013**, *2*, 1066–1071.

(59) van Stokkum, I. H. M.; Larsen, D. S.; van Grondelle, R. Global and Target Analysis of Time-Resolved Spectra. *BBA-Bioenergetics* **2004**, *1657*, 82–104.

(60) Henry, E. R.; Hofrichter, J. Singular Value Decomposition: Application to Analysis of Experimental Data. *Method Enzymol.* **1992**, *210*, 129–192.

(61) Snellenburg, J., J.; Laptenok, S.; Seger, R.; Mullen, K., M.; Van Stokkum, I., H.M. Glotaran: A Java-Based Graphical User Interface for the R Package Timp. *J. Stat. Software* **2012**, *49*, 1–22.

(62) Biskup, T.; Sommer, M.; Rein, S.; Meyer, D.L.; Kohlstädt, M.; Würfel, U.; Weber, S. Ordering of PCDTBT Revealed by Time-Resolved Electron Paramagnetic Resonance Spectroscopy of its Triplet Excitons. *Angew. Chem. Int. Ed.* **2015**, *54*, 7707–7710.

(63) Nohr, D.; Franz, S.; Rodriguez, R.; Paulus, B.; Essen, L.-O.; Weber, S.; Schleicher, E. Extended Electron-Transfer in Animal Cryptochromes Mediated by a Tetrad of Aromatic Amino Acids. *Biophys. J.* **2016**, *111*, 301–311.

(64) Lee, C.; Yang, W.; Parr, R. G. Development of the Colle-Salvetti Correlation-Energy Formula into a Functional of the Electron Density. *Phys. Rev. B* **1988**, *37*, 785–789.

(65) Becke, A. D. Density-Functional Thermochemistry. III. The Role of Exact Exchange. *J. Chem. Phys*. **1993**, *98*, 5648–5652.

(66) Yanai, T.; Tew, D. P.; Handy, N. C. A New Hybrid Exchange–Correlation Functional Using the Coulomb-Attenuating Method (CAM-B3LYP). *Chem. Phys. Lett*. **2004**, *393*, 51–57.

(67) Zhao, Y.; Truhlar, D. G. The Mo6 Suite of Density Functionals for Main Group Thermochemistry, Thermochemical Kinetics, Noncovalent Interactions, Excited States, and Transition Elements: Two New Functionals and Systematic Testing of Four Mo6-Class Functionals and 12 Other Functionals. *Theor. Chem. Acc.* **2008**, *120*, 215–241.

(68) Grimme, S. Semiempirical GGA-Type Density Functional Constructed with a Long-Range Dispersion Correction. *J. Comput. Chem.* **2006**, *27*, 1787–1799.

(69) Chai, J.-D.; Head-Gordon, M. Long-Range Corrected Hybrid Density Functionals with Damped Atom-Atom Dispersion Corrections. *Phys. Chem. Chem. Phys*. **2008**, *10*, 6615–6620.

(70) Perdew, J. P.; Burke, K.; Ernzerhof, M. Generalized Gradient Approximation Made Simple. *Phys. Rev. Lett.* **1996**, *77*, 3865–3868.

(71) Adamo, C.; Barone, V. Toward Reliable Density Functional Methods without Adjustable Parameters: The PBE0 Model. *J. Chem. Phys.* **1999**, *110*, 6158–6170.

(72) Vydrov, O. A.; Scuseria, G. E. Assessment of a Long-Range Corrected Hybrid Functional. *J. Chem. Phys*. **2006**, *125*, 234109.

(73) Vydrov, O. A.; Heyd, J.; Krukau, A. V.; Scuseria, G. E. Importance of Short-Range Versus Long-Range Hartree-Fock Exchange for the Performance of Hybrid Density Functionals. *J. Chem. Phys*. **2006**, *125*, 074106.

(74) Tomasi, J.; Mennucci, B.; Cammi, R. Quantum Mechanical Continuum Solvation Models. *Chem. Rev*. **2005**, *105*, 2999–3094.

(75) Frisch, M. J.; Trucks, G. W.; Schlegel, H. B.; Scuseria, G. E.; Robb, M. A.; Cheeseman, J. R.; Scalmani, G.; Barone, V.; Mennucci, B.; Petersson, G. A., et al. *Gaussian 09*, Revision D. 01; Gaussian, Inc.: Wallingford, CT, 2009.

(76) *DALTON. A Molecular Electronic Structure Program*. Release Dalton 2011, http://daltonprogram.org/ (accessed Oct 21, 2018).

(77) Ruud, K.; Schimmelpfennig, B.; Ågren, H. Internal and External Heavy-Atom Effects on Phosphorescence Radiative Lifetimes Calculated Using a Mean-Field Spin–Orbit Hamiltonian. *Chem. Phys. Lett*. **1999**, *310*, 215–221.

(78) Dong, Y.; Iagatti, A.; Foggi, P.; Zhao, J.; Mazzone, G.; Xu, K.; Ji, W.; Di Donato, M.; Russo, N. Bodipy-Squaraine Triads: Preparation and Study of the Intramolecular Energy Transfer, Charge Separation and Intersystem Crossing. *Dyes Pigments.* **2017**, *147*, 560–572.

(79) Suneesh, C. V.; Gopidas, K. R. Long-Lived Photoinduced Charge Separation in Flexible 9,10-Bis(Phenylethynyl) Anthracene−Phenothiazine Dyads. *J. Phys. Chem. C* **2009**, *113*, 1606–1614.

(80) Ajayakumar, G.; Gopidas, K. R. Long-Lived Photoinduced Charge Separation in New Ru (Bipyridine)$_3^{2+}$–Phenothiazine Dyads. *Photochem. Photobiol. Sci*. **2008**, *7*, 826–833.

(81) Hauck, M.; Turdean, R.; Memminger, K.; Schönhaber, J.; Rominger, F.; Müller, T. Luminescent, Redox-Active Diphenothiazine Dumbbells Expanded by Conjugated Arenes and Heteroarenes. *J. Org. Chem.* **2010**, *75*, 8591–8603.

(82) Wilkinson, F.; McGarvey, D.; Olea, A. Factors Governing the Efficiency of Singlet Oxygen Production During Oxygen Quenching of Singlet and Triplet States of Anthracene Derivatives in Cyclohexane Solution. *J. Am. Chem. Soc.* **1993**, *115*, 12144–12151.

(83) Xu, K.; Zhao, J.; Escudero, D.; Mahmood, Z.; Jacquemin, D. Controlling Triplet–Triplet Annihilation Upconversion by Tuning the PET in Aminomethyleneanthracene Derivatives. *J. Phys. Chem. C* **2015**, *119*, 23801–23812.

(84) Yildiz, A.; Reilley, C. N. The Mechanism of Intersystem Crossing for Some Substituted Aromatic Hydrocarbons. *Spectrosc. Lett*. **1968**, *1*, 335–343.

(85) Hunter, T.; Wyatt, R. Intersystem Crossing in Anthracene. *Chem. Phys. Lett*. **1970**, *6*, 221–224.

(86) Kanamaru, N. Radiationless Transition between Randomly Fluctuating Levels. S_1-T_2-T_1 Intersystem Crossing in Condensed Phase. *Bull. Chem. Soc. Jpn*. **1982**, *55*, 3093–3096.

(87) Suneesh, C. V.; Gopidas, K. R. Long-Lived Photoinduced Charge Separation Due to the Inverted Region Effect in 1,6-Bis(Phenylethynyl)Pyrene−Phenothiazine Dyad. *J. Phys. Chem. C* **2010**, *114*, 18725–18734.

(88) Zhu, M.; Ye, T.; Li, C.-G.; Cao, X.; Zhong, C.; Ma, D.; Qin, J.; Yang, C. Efficient Solution-Processed Nondoped Deep-Blue Organic Light-Emitting Diodes Based on Fluorene-Bridged Anthracene Derivatives Appended with Charge Transport Moieties. *J. Phys. Chem. C* **2011**, *115*, 17965–17972.

(89) Niladari Raju, M. V.; Mohanty, M. E.; Bangal, P. R.; Vaidya, J. R. Synthesis and Ultrafast Dynamics of a Donor–Acceptor–Donor Molecule Having Optoelectronic Properties. *J. Phys. Chem. C* **2015**, *119*, 8563–8575.

(90) Kowalski, J. A.; Casselman, M. D.; Kaur, A. P.; Milshtein, J. D.; Elliott, C. F.; Modekrutti, S.; Attanayake, N. H.; Zhang, N.; Parkin, S. R.; Risko, C. et al. A Stable Two-Electron-Donating Phenothiazine for Application in Nonaqueous Redox Flow Batteries. *J. Mater. Chem. A* **2017**, *5*, 24371–24379.

(91) Lockard, J. V.; Butler Ricks, A.; Co, D. T.; Wasielewski, M. R. Interrogating the Intramolecular Charge-Transfer State of a Julolidine−Anthracene Donor−Acceptor Molecule with Femtosecond Stimulated Raman Spectroscopy. *J. Phys. Chem. Lett.* **2010**, *1*, 215–218.

(92) Iwasaki, T.; Sawada, T.; Okuyama, M.; Kamada, H. The Photochemical Reaction of Aromatic Amines with Carbon Tetrachloride. *J. Phys. Chem.* **1978**, *82*, 371–372.

(93) Weber, S. Transient EPR. *eMagRes* **2017**, *6*, 255–270.

(94) Turro, N. J.; Kleinman, M. H.; Karatekin, E. Electron Spin Polarization and Time-Resolved Electron Paramagnetic Resonance: Applications to the Paradigms of Molecular and Supramolecular Photochemistry. *Angew. Chem. Int. Ed.* **2000**, *39*, 4436–4461.

(95) Kawai, A.; Shibuya, K. Electron Spin Dynamics in a Pair Interaction between Radical and Electronically-Excited Molecule as Studied by a Time-Resolved ESR Method. *J. Photochem. Photobio. C* **2006**, *7*, 89–103.

(96) Teki, Y.; Toichi, T.; Nakajima, S. π Topology and Spin Alignment in Unique Photoexcited Triplet and Quintet States Arising from Four Unpaired Electrons of an Organic Spin System. *Chem.–Eur. J*. **2006**, *12*, 2329–2336.

(97) Likhtenstein, G. I.; Ishii, K.; Nakatsuji, S. i. Dual Chromophore–Nitroxides: Novel Molecular Probes, Photochemical and Photophysical Models and Magnetic Materials. *Photochem. Photobiol*. **2007**, *83*, 871–881.

(98) Ogiwara, T.; Wakikawa, Y.; Ikoma, T. Mechanism of Intersystem Crossing of Thermally Activated Delayed Fluorescence Molecules. *J. Phys. Chem. A* **2015**, *119*, 3415–3418.

(99) Richert, S.; Bullard, G.; Rawson, J.; Angiolillo, P. J.; Therien, M. J.; Timmel, C. R. On the Importance of Electronic Symmetry for Triplet State Delocalization. *J. Am. Chem. Soc.* **2017**, *139*, 5301–5304.

(100) Richert, S.; Tait, C. E.; Timmel, C. R. Delocalisation of Photoexcited Triplet States Probed by Transient EPR and Hyperfine Spectroscopy. *J. Magn. Reson.* **2017**, *280*, 103–116.

(101) Anglos, D.; Bindra, V.; Kuki, A. Photoinduced Electron Transfer and Long-Lived Charge Separation in Rigid Peptide Architectures. *J. Chem. Soc., Chem. Commun.* **1994**, *2*, 213–215.

(102) Karpiuk, J. Photoinduced Electron Transfer in Malachite Green Lactone. *Phys. Chem. Chem. Phys.* **2003**, *5*, 1078–1090.

(103) Lee, S.-H.; Larsen, A. G.; Ohkubo, K.; Cai, Z.-L.; Reimers, J. R.; Fukuzumi, S.; Crossley, M. J. Long-Lived Long-Distance Photochemically Induced Spin-Polarized Charge Separation in β,β'-Pyrrolic Fused Ferrocene-Porphyrin-Fullerene Systems. *Chem. Sci.* **2012**, *3*, 257–269.

(104) van der Waals, J. H.; ter Maten, G. Zero-Field Splitting of the Lowest Triplet State of Some Aromatic Hydrocarbons: Calculation and Comparison with Experiment. *Mol. Phys.* **1964**, *8*, 301–318.

(105) Lhoste, J.-M.; Ptak, M.; Lexa, D. Le Premier État Triplet Phosphorescent de la Phénoxazine et de la Phénothiazine-I. Étude Par Résonance Paramagnétique Électronique. *J. Chim. Phys. Pcb*. **1968**, *65*, 1876–1888.

(106) Ghosh, H. N.; Sapre, A. V.; Palit, D. K.; Mittal, J. P. Picosecond Flash Photolysis Studies on Phenothiazine in Organic and Micellar Solution. *J. Phys. Chem. B* **1997**, *101*, 2315–2320.

TOC Graphic

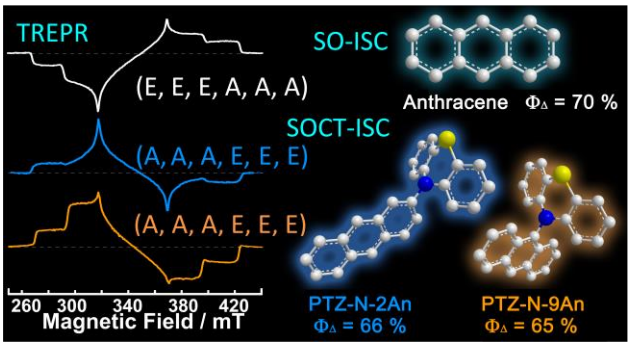
TREPR
(E, E, E, A, A, A)
(A, A, A, E, E, E)
(A, A, A, E, E, E)
260 300 340 380 420
Magnetic Field / mT
SO-ISC
Anthracene ΦΔ = 70 %
SOCT-ISC
PTZ-N-2An
ΦΔ = 66 %
PTZ-N-9An
ΦΔ = 65 %